

Associated production of H^\pm and W^\mp in high-energy e^+e^- collisions in the Minimal Supersymmetric Standard Model

Heather E. Logan^{1,*} and Shufang Su^{2,†}

¹*Theoretical Physics Department, Fermilab, PO Box 500, Batavia, Illinois 60510-0500, USA*

²*California Institute of Technology, Pasadena, California 91125, USA*

We study the associated production of the charged Higgs boson and W^\pm gauge boson in high energy e^+e^- collisions in the Minimal Supersymmetric Standard Model (MSSM). This associated production, which first arises at the one loop level, offers the possibility of producing the charged Higgs boson at the e^+e^- collider with mass more than half the center-of-mass energy, when the charged Higgs pair production is kinematically forbidden. We present analytic and numerical results for the cross section for $e^+e^- \rightarrow W^\pm H^\pm$ in the full MSSM, taking into account the previously uncalculated contributions from supersymmetric (SUSY) particles. We find that the contributions of the SUSY particles enhance the cross section over most of SUSY parameter space, especially when the SUSY particles are light, ~ 200 GeV. With favorable SUSY parameters, at small $\tan\beta$, this process can yield more than ten $W^\pm H^\mp$ events for $m_{H^\pm} \lesssim 350$ GeV in 500 fb^{-1} at a 500 GeV e^+e^- collider, or $m_{H^\pm} \lesssim 600$ GeV in 1000 fb^{-1} at a 1000 GeV collider. 80% left-handed polarization of the e^- beam improves these reaches to $m_{H^\pm} \lesssim 375$ GeV and $m_{H^\pm} \lesssim 670$ GeV, respectively.

PACS numbers: 12.60.Jv, 12.60.Fr, 14.80.Cp, 14.80.Ly

I. INTRODUCTION

Discovery of the heavy Higgs bosons H^0 , A^0 and H^\pm of the Minimal Supersymmetric Standard Model (MSSM)¹ poses a special challenge at future colliders. Run II of the Fermilab Tevatron, now in progress, has a limited reach for the neutral heavy MSSM Higgs bosons. It can detect the CP-even and CP-odd neutral Higgs bosons H^0 and A^0 if their masses are below about 150 GeV and $\tan\beta$ (the ratio of the two Higgs vacuum expectation values) is large, so that the couplings of H^0 and A^0 to b quarks are enhanced [3, 4, 5, 6]. For the charged Higgs boson H^\pm , no sensitivity is expected via direct production at the Tevatron unless QCD and SUSY effects conspire to enhance the cross section [7]; however, H^\pm can be discovered in top quark decays for $m_{H^\pm} \lesssim m_t$ and large $\tan\beta$ [5, 8]. The CERN Large Hadron Collider (LHC) has a much greater reach for heavy MSSM Higgs boson discovery at moderate to large values of $\tan\beta$. H^0 and A^0 can be discovered with decays to τ pairs for $\tan\beta \gtrsim 10$ for a CP-odd Higgs mass of $m_{A^0} = 250$ GeV ($\tan\beta \gtrsim 17$ for $m_{A^0} = 500$ GeV) [9, 10]. The charged MSSM Higgs boson H^\pm can be discovered in $gb \rightarrow tH^+$ with $H^+ \rightarrow \tau\nu$ for virtually the same $\tan\beta$ values [10, 11]. The absence of a Higgs boson discovery at the CERN LEP-2 experiments implies that $0.5 < \tan\beta < 2.4$ and $m_{A^0} < 91.9$ GeV are excluded at 95% confidence level [12]. This leaves a wedge-shaped region of parameter space at moderate $\tan\beta$ in which the heavy MSSM Higgs bosons will not be discovered at the

LHC. At a future high energy e^+e^- linear collider (LC), the heavy Higgs bosons will be produced in pairs, if it is kinematically allowed. The dominant production modes are $e^+e^- \rightarrow H^0 A^0$ and $e^+e^- \rightarrow H^+ H^-$; for experimental studies see Refs. [13, 14]. These production modes are kinematically allowed only if $m_{H^0} + m_{A^0} < \sqrt{s}$ and $2m_{H^\pm} < \sqrt{s}$, respectively, where \sqrt{s} is the center-of-mass energy of the LC.² At large m_{A^0} , $m_{A^0} \simeq m_{H^0} \simeq m_{H^\pm}$ up to mass splittings of order m_Z^2/m_{A^0} , so that the pair-production modes are kinematically allowed only if $m_{A^0} \lesssim 0.5\sqrt{s}$. In particular, the pair-production modes are limited to $m_{A^0} \lesssim 250$ GeV ($m_{A^0} \lesssim 500$ GeV) at a LC with $\sqrt{s} = 500$ GeV ($\sqrt{s} = 1000$ GeV).

By contrast, the discovery of the light MSSM Higgs boson h^0 , which typically has properties similar to those of the SM Higgs boson, is much more certain. At Run II of the Tevatron, discovery of h^0 at the 5σ level is possible for $m_{h^0} \lesssim 120$ GeV if 15 fb^{-1} of integrated luminosity can be collected and the detectors perform as expected [5]. This covers a large fraction of the MSSM parameter space left unexcluded after LEP-2 [12]. At the LHC, discovery of h^0 is virtually guaranteed over all of the MSSM parameter space [9]. Enough h^0 events are expected in a number of different production and decay modes to allow the measurement of various combinations of h^0 partial widths with precisions on the order of 15% [15]. At the LC, h^0 will be copiously produced. The promise of the LC for making precision measurements of the couplings of h^0 at the few-percent level has been well documented [16, 17, 18]. If the MSSM Higgs sector is not too far into the decoupling limit [19], in which the

*Electronic address: logan@fnal.gov

†Electronic address: shufang@theory.caltech.edu

¹ For a pedagogical introduction to the MSSM Higgs sector, see Refs. [1, 2].

² The pair production of scalars is p -wave suppressed near threshold, so in practice the Higgs mass reach in these modes is likely to be somewhat below the kinematic limit.

heavy Higgs bosons become increasingly heavy and the couplings of h^0 to SM particles approach their SM values (so that h^0 behaves like the SM Higgs boson), the LC measurements of h^0 couplings can be used to distinguish h^0 from the SM Higgs boson and to extract MSSM parameters [20]. One finds $\geq 2\sigma$ deviations from the SM typically for $m_{A^0} \lesssim 600$ GeV [16, 20].³

While in the decoupling limit the couplings of h^0 become increasingly insensitive to the MSSM parameters, the couplings of the heavy Higgs bosons exhibit no such decoupling; rather, they are always sensitive to the MSSM parameters. Further, the measurements of the masses and couplings of the heavy Higgs bosons in addition to those of h^0 allow one to place orthogonal constraints on the parameters of the MSSM Higgs sector. Thus, measurements of the properties of the heavy MSSM Higgs bosons are very valuable, especially in the decoupling limit.

In this paper we consider the production of one of the heavy Higgs bosons alone or in association with lighter SM particles at the LC. While the cross sections for such production modes are typically very small, they offer the possibility of extending the reach of the LC to higher values of $m_{A^0, H^0, H^\pm} \gtrsim 0.5\sqrt{s}$. Single heavy Higgs boson production has been studied before in the literature via a number of different processes, which we summarize here. Because detailed experimental studies of almost all of these processes are unavailable, we choose an optimistic standard of detectability to be 10 heavy Higgs boson production events in the LC data sample. We assume data samples of 500 fb^{-1} at $\sqrt{s} = 500$ GeV and 1000 fb^{-1} at $\sqrt{s} = 1000$ GeV. For neutral Higgs boson production, this standard corresponds to a cross section of 0.02 fb at $\sqrt{s} = 500$ GeV (0.01 fb at $\sqrt{s} = 1000$ GeV). For the charged Higgs boson production, we may add together the cross sections for H^+ and H^- production. Thus our standard corresponds to a cross section for production of a charged Higgs boson of one sign of 0.01 fb at $\sqrt{s} = 500$ GeV (0.005 fb at $\sqrt{s} = 1000$ GeV). We assume unpolarized e^- beams unless otherwise specified; we always assume that the e^+ beams are unpolarized.

The heavy CP-even neutral Higgs boson H^0 can be produced via the same processes as the SM Higgs boson, *i.e.*, Higgsstrahlung, $e^+e^- \rightarrow ZH^0$; W -boson fusion, $e^+e^- \rightarrow \nu\bar{\nu}H^0$; and Z -boson fusion, $e^+e^- \rightarrow e^+e^-H^0$. However, the cross sections for these production processes are suppressed relative to the corresponding SM Higgs production cross sections by $\cos^2(\beta - \alpha)$, where α is the mixing angle that diagonalizes the CP-even neutral Higgs boson mass-squared matrix. In the decoupling limit [19], $\cos^2(\beta - \alpha) \propto m_Z^4/m_{A^0}^4$, so these cross sections quickly become very small as m_{A^0} increases. At a

500 GeV LC, ZH^0 production can provide some reach beyond $m_{H^0} \simeq 0.5\sqrt{s} = 250$ GeV at low $\tan\beta$. Using the program FeynHiggsXS [22], which includes the full Feynman-diagrammatic corrections to this process at the one-loop level as well as two-loop corrections to the Higgs masses and mixing, we find that ZH^0 production yields a cross section above 0.02 fb for $m_{H^0} \lesssim 385$ GeV at $\tan\beta = 2.5$ ($m_{H^0} \lesssim 325$ GeV at $\tan\beta = 10$). At a 1000 GeV LC, the cross section for ZH^0 production is tiny, below about 0.005 fb for $\tan\beta \gtrsim 2.5$ and $m_{H^0} > 500$ GeV. At $\sqrt{s} = 500$ GeV, the cross section for SM Higgs boson production through W -boson fusion is smaller than that for SM Higgs boson production via $e^+e^- \rightarrow ZH^0$ for $m_{H^0} \gtrsim 165$ GeV (see, *e.g.*, Ref. [18]); thus in the MSSM we do not expect the W -boson fusion process to improve the reach for H^0 over ZH^0 production at this center-of-mass energy. At $\sqrt{s} = 1000$ GeV, however, the SM W -boson fusion cross section is considerably larger than the SM ZH^0 production cross section all the way up to the kinematic limit. This process yields a cross section above 0.02 fb for $m_{H^0} \lesssim 550$ GeV at $\tan\beta = 2.5$.⁴ Finally, the Z -boson fusion cross section is always about a factor of ten smaller than the W -boson fusion cross section, so we do not expect it to be useful here.

In addition to the unsuppressed but kinematically limited production mode $e^+e^- \rightarrow H^0A^0$, the heavy CP-odd neutral Higgs boson can also be produced in association with the light h^0 , via $e^+e^- \rightarrow h^0A^0$. As above, the cross section for this production mode is suppressed by $\cos^2(\beta - \alpha)$. At a 500 GeV LC, this process may provide some reach for $m_{A^0} > 250$ GeV at low $\tan\beta$; using FeynHiggsXS [22] we find that it yields a cross section above 0.02 fb for $m_{A^0} \lesssim 355$ GeV at $\tan\beta = 2.5$ ($m_{A^0} \lesssim 270$ GeV at $\tan\beta = 10$). At a 1000 GeV LC, the cross section is below 0.02 fb for $\tan\beta \gtrsim 2.5$ and $m_{A^0} > 500$ GeV.

The heavy MSSM Higgs bosons can also be produced in association with pairs of third-generation fermions: $e^+e^- \rightarrow b\bar{b}H^0$, $b\bar{b}A^0$, $\tau^-\nu H^+$, and $t\bar{b}H^+$. The cross sections for the first three of these processes are strongly enhanced at large $\tan\beta$, and the fourth is enhanced at both large and small $\tan\beta$.⁵ The cross sections for all four processes fall rapidly with increasing m_{A^0} . At a 500 GeV LC, the process $e^+e^- \rightarrow b\bar{b}H^0$ can provide some reach for $m_{H^0} > 250$ GeV at large $\tan\beta$; it yields a cross section of 0.1 fb or greater for $m_{H^0} \lesssim 350$ GeV at $\tan\beta = 50$ ($m_{H^0} \lesssim 300$ GeV at $\tan\beta = 30$) [25, 26]⁶. The process $e^+e^- \rightarrow b\bar{b}A^0$ yields cross sections below 0.1

³ A subset of the h^0 couplings can also be measured with similar precision at a LC operating as a $\gamma\gamma$ collider, leading again to $\geq 2\sigma$ deviations from the SM typically for $m_{A^0} \lesssim 600$ GeV [21].

⁴ These results for $e^+e^- \rightarrow \nu\bar{\nu}H^0$ are based on the α_{eff} approximation from the program subhpoldm [23]. A full Feynman-diagrammatic calculation of the radiative corrections to this process is not yet available.

⁵ The first two processes are useful for measuring $\tan\beta$ at large $\tan\beta$ and low m_{A^0} [24].

⁶ Results were not given in Refs. [25, 26] for cross sections smaller than 0.1 fb. Presumably, the reach in m_{H^0} is somewhat larger at a cross section of 0.02 fb.

fb for $m_{A^0} > 250$ GeV [25, 26]. At a 1000 GeV LC, neither $e^+e^- \rightarrow b\bar{b}H^0$ nor $b\bar{b}A^0$ yields a cross section above 0.1 fb for $m_{H^0, A^0} > 500$ GeV [25]. At a 500 GeV LC, the process $e^+e^- \rightarrow \tau^-\bar{\nu}H^+$ yields a cross section above 0.01 fb for $m_{H^\pm} \lesssim 275$ GeV at large $\tan\beta \sim 40$, while $e^+e^- \rightarrow \bar{t}bH^+$ yields a cross section above 0.01 fb for $m_{H^\pm} \lesssim 260$ GeV for low (~ 1.5) or high (~ 40) values of $\tan\beta$ [27] (see also Refs. [25, 28]). At a 1000 GeV LC, the process $e^+e^- \rightarrow \tau^-\bar{\nu}H^+$ yields a cross section above 0.005 fb for $m_{H^\pm} \lesssim 520$ GeV at large $\tan\beta \sim 40$, while $e^+e^- \rightarrow \bar{t}bH^+$ yields a cross section above 0.005 fb for $m_{H^\pm} \lesssim 550$ GeV for low (~ 1.5) or high (~ 40) $\tan\beta$ [27] (see also Ref. [25]). If the e^+e^- LC is converted into a photon collider through Compton backscattering of intense laser beams, similar single Higgs production processes are possible with cross sections for $m_{H^\pm} > \sqrt{s}/2$ typically larger than those in e^+e^- collisions [29]. At a 1000 GeV parent e^+e^- machine, $\gamma\gamma \rightarrow \tau^-\bar{\nu}H^+$ yields a cross section above 0.005 fb for m_{H^\pm} up to almost 700 GeV at large $\tan\beta \simeq 30$ [29].

At a photon collider, the neutral heavy Higgs bosons H^0 and A^0 can be singly produced in the s -channel through their loop-induced couplings to photon pairs. This process currently appears to be the most promising for detecting H^0 and A^0 with masses above $\sqrt{s}/2$ and $\tan\beta$ values in the LHC wedge region [30, 31, 32]. In particular, a recent realistic simulation [30] shows that a 630 GeV e^+e^- LC running in $\gamma\gamma$ mode for three years would allow H^0 , A^0 detection over a large fraction of the LHC wedge region for m_{A^0} up to the photon-photon energy limit of ~ 500 GeV. At a 1000 GeV LC, the mass reach is likely to be above 600 GeV [31].

Production of charged Higgs bosons at a photon collider via $\gamma\gamma \rightarrow W^+H^-$ at the one-loop level has been studied in the non-supersymmetric two Higgs doublet model (2HDM) and the full MSSM in Ref. [33]. If 1000 fb $^{-1}$ of e^+e^- luminosity is devoted to $\gamma\gamma$ collisions at $\sqrt{s_{ee}} = 1000$ GeV, a ten-event discovery of H^\pm in the 2HDM is possible for $m_{H^\pm} \lesssim 570$ GeV at $\tan\beta = 2$; the cross section falls with increasing $\tan\beta$. In the full MSSM with light superparticles the cross section is enhanced, and this mode provides a ten-event discovery reach for m_{H^\pm} above 600 GeV at $\tan\beta = 2$ ($m_{H^\pm} \lesssim 520$ GeV at $\tan\beta = 6$) [33].

Single heavy MSSM Higgs bosons can be produced at the e^+e^- LC through a number of loop-induced processes as well. The process $e^+e^- \rightarrow ZA^0$ is forbidden at tree-level but present at one loop. A significant contribution to this process comes from the loop-induced A^0ZZ vertex, computed in Ref. [34]. The full cross section for $e^+e^- \rightarrow ZA^0$ has been calculated in both the 2HDM [35] and in the full MSSM [36]. In the 2HDM the cross section is very small, about 0.003 fb 7 for $\tan\beta \simeq 1.5$ and

$\sqrt{s} = 500$ GeV, and falls rapidly with increasing $\tan\beta$ [35]. In the full MSSM, light charginos and sleptons with masses of order 200 GeV can enhance the cross section by an order of magnitude or more; this leads to a cross section for $e^+e^- \rightarrow ZA^0$ at a 500 GeV LC larger than 0.02 fb 8 for $m_{A^0} \lesssim 270$ GeV for a wide range of $\tan\beta$ values [36]. This enhancement disappears once the chargino and slepton masses exceed about 500 GeV. Similarly, the process $e^+e^- \rightarrow \gamma A^0$ was considered in Refs. [35, 38, 39]. At a 500 GeV machine, even including the enhancement of the cross section from SUSY contributions, the cross section is below 0.02 fb for $m_{A^0} > 250$ GeV at $\tan\beta = 2$, and falls rapidly with increasing $\tan\beta$ [38]. At higher \sqrt{s} the situation is similarly unpromising for $\tan\beta > 2$ [39].

The similar process $e^+e^- \rightarrow W^+H^-$ is also forbidden at tree level but present at one-loop. A significant contribution to this process comes from the loop-induced W^+H^-Z and $W^+H^-\gamma$ vertices. The contributions to these vertices from top/bottom quark loops [40] and gauge and Higgs boson loops [41] have been computed in the 2HDM. The full MSSM contributions to these vertices have been computed in Ref. [42]; the contributions from top/bottom squark loops are also given in Ref. [40]. The loop-induced W^+H^-Z vertex has also been computed numerically in the full MSSM in Ref. [43].

The loop-induced $W^+H^-\gamma$ coupling leads to the process $e^-\gamma \rightarrow \nu H^-$. The cross section for this process has been computed in the 2HDM in Ref. [44]. The cross section is relatively independent of m_{H^\pm} all the way up to threshold for $e^-\gamma$ center-of-mass energies of either 450 or 900 GeV. However, the cross section is quite small, typically below 0.05 fb for $\tan\beta \geq 1.5$, and falls rapidly with increasing $\tan\beta$ [44]. With a typical $e^-\gamma$ luminosity of 100 fb $^{-1}$ [45], a cross section of at least 0.1 fb would be required to obtain 10 H^- events.

The full cross section for $e^+e^- \rightarrow W^+H^-$ has been calculated in the non-supersymmetric 2HDM in Refs. [46, 47, 48]. If one imposes the MSSM relations on the 2HDM Higgs sector, then the cross section at a 500 GeV LC is above 0.01 fb for $m_{H^\pm} \lesssim 380$ GeV and $\tan\beta = 2$; it falls rapidly with increasing $\tan\beta$ [48]. If the MSSM constraint on the Higgs sector is relaxed, as in Ref. [47], then the $e^+e^- \rightarrow W^+H^-$ cross section can be enhanced in some regions of 2HDM parameter space with $\tan\beta \gtrsim 3$ due to large triple-Higgs couplings. This enhancement is limited to a little less than an order of magnitude by the requirement that the Higgs self-coupling constants remain perturbative. The resulting cross sections reach a maximum of about 0.05 fb 9 for $m_{H^\pm} \gtrsim 250$ GeV at $\tan\beta \simeq 4$, and fall rapidly with increasing $\tan\beta$ and increasing m_{H^\pm} [47]. Similar results were obtained in

omitted in Refs. [35, 36] [37].

⁸ We have again taken into account the additional factor of 1/4 from the average over the e^+e^- polarizations [37].

⁹ Ref. [47] presents cross sections for 100% polarized e^- and e^+ beams; we quote the unpolarized cross section here.

⁷ We have taken into account an additional factor of 1/4 due to the average over the initial e^+e^- polarizations that was accidentally

Ref. [46].

In this paper we compute the cross section for $e^+e^- \rightarrow W^+H^-$ in the full MSSM. We present analytic formulae for the matrix elements and numerical results for the cross section as a function of the MSSM parameters. We find that the contributions of the SUSY particles enhance the cross section over most of SUSY parameter space, especially when the SUSY particles are light, with masses of order 200 GeV. The largest contributions to the cross section from the SUSY sector come from diagrams involving charginos/neutralinos and top/bottom squarks. We also find that left-handed polarization of the e^- beams leads to an order 50% enhancement of the cross section. Throughout this paper we present cross sections for the single process $e^+e^- \rightarrow W^+H^-$; these numbers should be doubled to find the combined cross sections for this process plus its charge conjugate.

This paper is organized as follows. In Sec. II we introduce our formalism for the matrix elements and cross section. In Sec. III we display the relevant SUSY diagrams and review the renormalization procedure. In Sec. IV we present our numerical results. Sec. V is reserved for our conclusions. The matrix elements for the 2HDM and SUSY diagrams are collected in the appendix.

II. FORMALISM

Following the notation of Ref. [46], the matrix element \mathcal{M} for $e^+e^- \rightarrow W^+H^-$ can be decomposed into six independent matrix elements \mathcal{A}_i and their corresponding coefficients \mathcal{M}_i :

$$\mathcal{M} = \sum_{i=1}^6 \mathcal{M}_i \mathcal{A}_i. \quad (1)$$

The six matrix elements are defined as,

$$\mathcal{A}_1 = \bar{v}(p_2) \ell^*(k_1) \frac{1 + \gamma_5}{2} u(p_1)$$

and

$$\frac{d\sigma(e_R^+ e_L^- \rightarrow W^+ H^-)}{d\cos\theta} = \frac{\kappa}{32\pi s} \left[2s|\mathcal{M}_2|^2 - \frac{(m_{H^\pm}^2 m_W^2 - tu)}{4m_W^2} \left\{ (m_W^2 - t)^2 |\mathcal{M}_4|^2 + (m_W^2 - u)^2 |\mathcal{M}_6|^2 \right. \right. \\ \left. \left. + 4(m_W^2 - t) \text{Re}[\mathcal{M}_2 \mathcal{M}_4^*] + 4(m_W^2 - u) \text{Re}[\mathcal{M}_2 \mathcal{M}_6^*] + 2(tu - m_W^2 s - m_W^2 m_{H^\pm}^2) \text{Re}[\mathcal{M}_4 \mathcal{M}_6^*] + 4|\mathcal{M}_2|^2 \right\} \right], \quad (6)$$

$$\frac{d\sigma(e_L^+ e_R^- \rightarrow W^+ H^-)}{d\cos\theta} = \frac{\kappa}{32\pi s} \left[2s|\mathcal{M}_1|^2 - \frac{(m_{H^\pm}^2 m_W^2 - tu)}{4m_W^2} \left\{ (m_W^2 - t)^2 |\mathcal{M}_3|^2 + (m_W^2 - u)^2 |\mathcal{M}_5|^2 \right. \right. \\ \left. \left. + 4(m_W^2 - t) \text{Re}[\mathcal{M}_1 \mathcal{M}_3^*] + 4(m_W^2 - u) \text{Re}[\mathcal{M}_1 \mathcal{M}_5^*] + 2(tu - m_W^2 s - m_W^2 m_{H^\pm}^2) \text{Re}[\mathcal{M}_3 \mathcal{M}_5^*] + 4|\mathcal{M}_1|^2 \right\} \right]. \quad (7)$$

Here $s = (p_1 + p_2)^2$ and $\kappa = 2|\vec{k}_1|/\sqrt{s}$ is given by:

$$\kappa^2 = \left[1 - \frac{(m_{H^\pm} + m_W)^2}{s} \right] \left[1 - \frac{(m_{H^\pm} - m_W)^2}{s} \right]. \quad (8)$$

$$\begin{aligned} \mathcal{A}_2 &= \bar{v}(p_2) \ell^*(k_1) \frac{1 - \gamma_5}{2} u(p_1) \\ \mathcal{A}_3 &= \bar{v}(p_2) k_1 \frac{1 + \gamma_5}{2} u(p_1) (p_1 \cdot \epsilon^*(k_1)) \\ \mathcal{A}_4 &= \bar{v}(p_2) k_1 \frac{1 - \gamma_5}{2} u(p_1) (p_1 \cdot \epsilon^*(k_1)) \\ \mathcal{A}_5 &= \bar{v}(p_2) k_1 \frac{1 + \gamma_5}{2} u(p_1) (p_2 \cdot \epsilon^*(k_1)) \\ \mathcal{A}_6 &= \bar{v}(p_2) k_1 \frac{1 - \gamma_5}{2} u(p_1) (p_2 \cdot \epsilon^*(k_1)), \end{aligned} \quad (2)$$

where ϵ^* is the polarization vector of the W^+ boson, p_1 and p_2 are the incoming momenta of the initial e^- and e^+ , respectively, and k_1 is the outgoing momentum of the W^+ .

For convenience we define two additional matrix elements, \mathcal{A}_7 and \mathcal{A}_8 :

$$\begin{aligned} \mathcal{A}_7 &= i\varepsilon^{\alpha\mu\beta\gamma} \bar{v}(p_2) \gamma_\mu \frac{1 + \gamma_5}{2} u(p_1) \epsilon_\alpha^* k_{1\beta} k_{2\gamma} \\ \mathcal{A}_8 &= i\varepsilon^{\alpha\mu\beta\gamma} \bar{v}(p_2) \gamma_\mu \frac{1 - \gamma_5}{2} u(p_1) \epsilon_\alpha^* k_{1\beta} k_{2\gamma}, \end{aligned} \quad (3)$$

where $k_2 = p_1 + p_2 - k_1$ is the outgoing momentum of the H^- and $\varepsilon^{\alpha\mu\beta\gamma}$ is the totally antisymmetric tensor, with $\varepsilon^{0123} = 1$. \mathcal{A}_7 and \mathcal{A}_8 can be expressed in terms of $\mathcal{A}_1 - \mathcal{A}_6$ as follows:

$$\begin{aligned} \mathcal{A}_7 &= \mathcal{A}_1(t - u)/2 + \mathcal{A}_3 - \mathcal{A}_5 \\ \mathcal{A}_8 &= \mathcal{A}_2(u - t)/2 - \mathcal{A}_4 + \mathcal{A}_6, \end{aligned} \quad (4)$$

where $t = (p_1 - k_1)^2$ and $u = (p_1 - k_2)^2$.

From the form of these matrix elements, one immediately sees that the cross sections for like polarizations of e^+ and e^- are zero:

$$\frac{d\sigma(e_R^+ e_L^- \rightarrow W^+ H^-)}{d\cos\theta} = \frac{d\sigma(e_L^+ e_R^- \rightarrow W^+ H^-)}{d\cos\theta} = 0. \quad (5)$$

For unlike polarizations of e^+ and e^- , the cross sections are given in terms of the six basic matrix elements by:

The unpolarized cross section is obtained by averaging

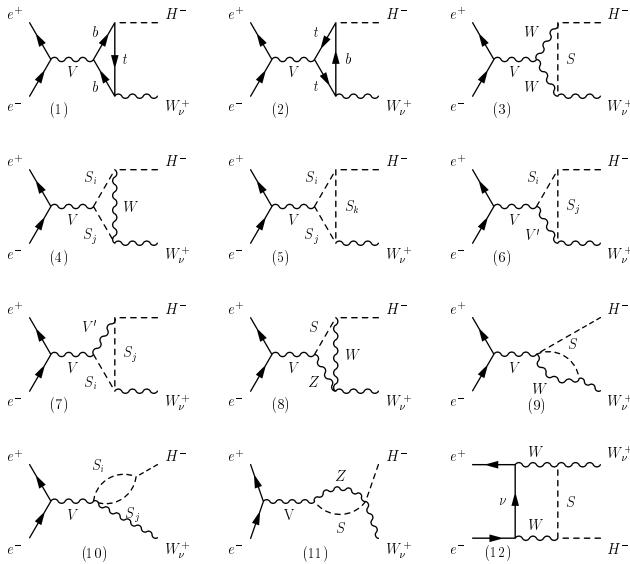


FIG. 1: Feynman diagrams for the 2HDM contributions to $e^+e^- \rightarrow W^+H^-$. Here S_i , $S_{i,j,k}$ denote Higgs and Goldstone bosons, $V = \gamma$, Z , and $V' = Z$, W^\pm .

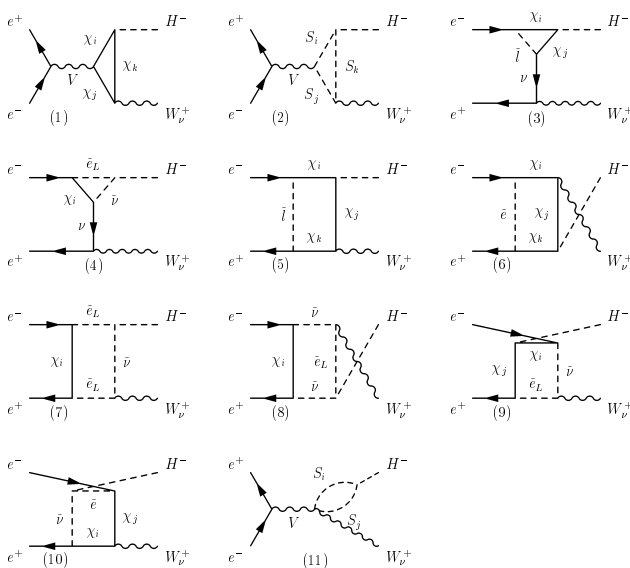


FIG. 2: Feynman diagrams for the SUSY contributions to $e^+e^- \rightarrow W^+H^-$. Here $\chi_{i,j,k}$ denote charginos and neutralinos, $S_{i,j,k}$ denote squarks and sleptons, and $V = \gamma$, Z .

over the four possible initial combinations of e^+e^- polarizations.

III. RENORMALIZATION

The diagrams contributing to $e^+e^- \rightarrow W^+H^-$ in the 2HDM are shown in Fig. 1 [46]. We show the additional SUSY diagrams in Fig. 2. There are also W^-H^- and G^-H^- mixing self-energy diagrams that involve SM

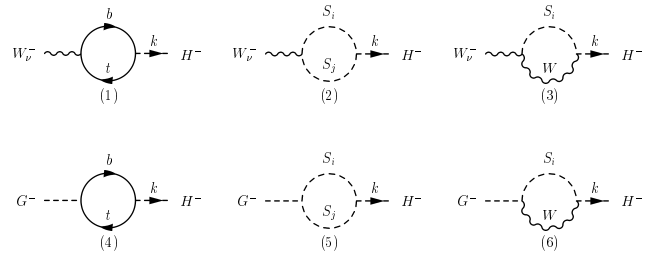


FIG. 3: Feynman diagrams for the 2HDM contributions to W^-H^- and G^-H^- mixing self-energies. Here $S_i = h^0, H^0$ and $S_j = H^\pm, G^\pm$.

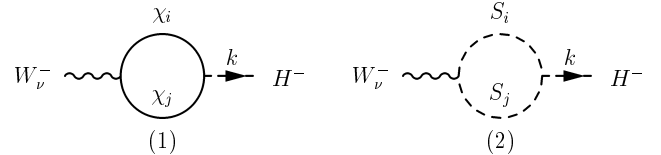


FIG. 4: Feynman diagrams for the SUSY contributions to W^-H^- and G^-H^- mixing self-energies. Here $\chi_{i,j}$ denote charginos and neutralinos and $S_{i,j}$ denote squarks and sleptons.

fermions, gauge and Higgs bosons (Fig. 3), and SUSY particles (Fig. 4). These mixing self-energies, together with the counterterms, contribute to $e^+e^- \rightarrow W^+H^-$ via the diagrams in Fig. 5.

We neglect all diagrams that are proportional to the electron Yukawa coupling. We also neglect the diagrams shown in Fig. 6:

- These two diagrams are proportional to m_e either through the electron Yukawa coupling or through the factor of m_e obtained via the equation of motion of the incoming electron. In particular, the vector boson–Higgs mixing is proportional to $k_\mu^V = p_{1\mu} + p_{2\mu}$, which gives m_e when acting on the $V_\mu \bar{e} \gamma^\mu e$ vertex.
- This diagram is zero because the W^-H^- mixing self-energy is proportional to $k_{1\nu}$, and $k_1 \cdot \epsilon^* = 0$.
- We will set the renormalized tadpoles to zero below, so that this diagram does not contribute. (Note that the A^0 and G^0 tadpoles are zero automatically due to CP conservation.)
- This diagram is purely real and is canceled by the G^-H^- mixing counterterm, as discussed below.

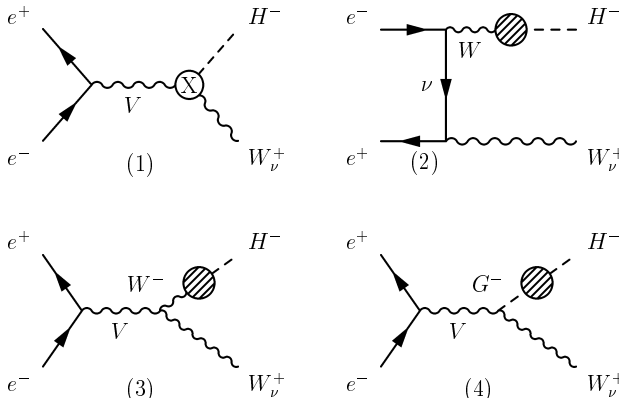


FIG. 5: Feynman diagrams for the contributions to $e^+e^- \rightarrow W^+H^-$ through the counter terms and the W^-H^- and G^-H^- mixing self-energies. The “X” in diagram 1 denotes the counter term for the γW^+H^- and ZW^+H^- vertex, and the blob in diagrams 2-4 denotes the renormalized W^-H^- and G^-H^- mixing.

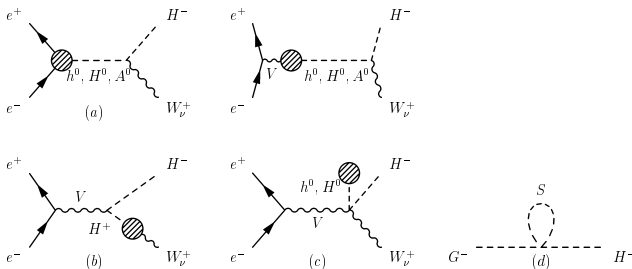


FIG. 6: Contributions to $e^+e^- \rightarrow W^+H^-$ that we neglect.

We evaluate the one-loop process $e^+e^- \rightarrow W^+H^-$ in the ’t Hooft–Feynman gauge using dimensional regularization. Using dimensional reduction yields the same result for this process. Diagrams that contain closed loops of chiral fermions may give rise to inconsistencies in the treatment of γ^5 in naïve dimensional regularization [49, 50]. We have checked that this does not happen in the one-loop $e^+e^- \rightarrow W^+H^-$ diagrams by computing the terms involving γ^5 in the diagrams with closed fermion loops using the ’t Hooft-Veltman rules [49, 51]. It was shown in Ref. [49] that this prescription yields a consistent formulation of dimensional regularization even if γ^5 couplings are present. (For a pedagogical discussion see Ref. [52].) We find that in this process the ’t Hooft-Veltman rules yield the same result as naïve dimensional regularization, so that no inconsistencies arise.

We follow the on-shell renormalization formalism developed by Dabelstein [53] for the MSSM gauge and Higgs sectors. The one-particle-irreducible (1PI) tadpole diagrams for h^0 and H^0 are given by $-iT_h$ and $-iT_H$, respectively. Including the tadpole counterterms, the renormalized tadpoles are given by:

$$\hat{T}_h = T_h + \delta t_h, \quad \hat{T}_H = T_H + \delta t_H. \quad (9)$$

The 1PI two-point function for W^+H^+ mixing is de-

fined as $-ik_\mu \Sigma_{W^+H^+}(k^2)$, where k is the incoming momentum of the W_μ^+ , and H^+ is outgoing.¹⁰ The conjugate two-point function, with W^- incoming and H^- outgoing, is given by $+ik_\mu \Sigma_{W^-H^+}(k^2)$, where again k is the incoming momentum of the W_μ^- . The renormalized two-point function for W^+H^+ mixing is obtained by adding the counterterm:

$$\hat{\Sigma}_{W^+H^+}(k^2) = \Sigma_{W^+H^+}(k^2) - m_W \sin \beta \cos \beta \left(\delta Z_{H_1} - \delta Z_{H_2} - \frac{\delta v_1}{v_1} + \frac{\delta v_2}{v_2} \right), \quad (10)$$

where δZ_{H_1} and δZ_{H_2} renormalize the two Higgs doublet fields H_1 and H_2 and δv_1 and δv_2 renormalize the two Higgs vacuum expectation values [53]:

$$H_i \rightarrow Z_{H_i}^{1/2} H_i; \quad v_i \rightarrow Z_{H_i}^{1/2} (v_i - \delta v_i), \quad (11)$$

and $Z_{H_i} = 1 + \delta Z_{H_i}$.

The 1PI two-point function for G^+H^+ mixing is defined as $+i\Sigma_{G^+H^+}(k^2)$, where k is the incoming momentum of the G^+ , and H^+ is outgoing. The conjugate two-point function, with G^- incoming and H^- outgoing, is the same. The renormalized two-point function for G^+H^+ mixing, $\hat{\Sigma}_{G^+H^+}(k^2)$, is fixed in terms of $\hat{\Sigma}_{W^+H^+}(k^2)$ due to the Slavnov-Taylor identity (see, *e.g.*, Refs. [54, 55] for details):

$$k^2 \hat{\Sigma}_{W^+H^+}(k^2) - m_W \hat{\Sigma}_{G^+H^+}(k^2) = 0. \quad (12)$$

Finally, there are two vertex counterterms for $\gamma_\mu W_\nu^+ H^-$ and $Z_\mu W_\nu^+ H^-$ (all particles outgoing). These are given by $-iem_W \sin \beta \cos \beta \delta c g_{\mu\nu}$ and $+ies_W m_Z \sin \beta \cos \beta \delta c g_{\mu\nu}$, respectively. Here $\delta c \equiv (\delta Z_{H_1} - \delta Z_{H_2} - \delta v_1/v_1 + \delta v_2/v_2)$ and s_W denotes the sine of the weak mixing angle. Note that δc is fixed in terms of the W^+H^+ mixing counterterm, Eq. 10.

We need impose only the following two renormalization conditions.¹¹ First, the renormalized tadpoles in Eq. 9 are set to zero. Second, the real part of the renormalized W^+H^+ mixing is set to zero when H^+ is on mass shell:

$$\text{Re } \hat{\Sigma}_{W^+H^+}(m_{H^\pm}^2) = 0. \quad (13)$$

This fixes the following combination of counterterms:

$$\begin{aligned} m_W \sin \beta \cos \beta \left(\delta Z_{H_1} - \delta Z_{H_2} - \frac{\delta v_1}{v_1} + \frac{\delta v_2}{v_2} \right) \\ = \text{Re } \Sigma_{W^+H^+}(m_{H^\pm}^2), \end{aligned} \quad (14)$$

¹⁰ We use the convention $\mathcal{D}_\mu = \partial_\mu + ieA_\mu$. Ref. [46] uses the opposite convention, so our matrix elements should differ from theirs by a sign.

¹¹ Because the process $e^+e^- \rightarrow W^+H^-$ is zero at tree level, the renormalization procedure is greatly simplified and many renormalization conditions, such as that for $\tan \beta$, need not be imposed.

which appears in the $\gamma W^+ H^-$ and $Z W^+ H^-$ vertex counterterms. Applying the Slavnov-Taylor identity (Eq. 12) at $k^2 = m_{H^\pm}^2$, this condition also fixes $\text{Re } \hat{\Sigma}_{G+H^+}(m_{H^\pm}^2) = 0$. In addition, since the counterterms are purely real, we have from Eq. 12:

$$\text{Im } \Sigma_{G+H^+}(m_{H^\pm}^2) = \frac{m_{H^\pm}^2}{m_W} \text{Im } \Sigma_{W^+H^+}(m_{H^\pm}^2), \quad (15)$$

so that diagrams 3 and 4 of Fig. 4 and diagram (d) of Fig. 6 need not be calculated. As a check of our calculation we have verified Eq. 15 explicitly, including the full MSSM contributions.

Explicit results for $\Sigma_{W^+H^+}(p^2)$ are given in the appendix. The real part of $\Sigma_{W^+H^+}(m_{H^\pm}^2)$ fixes the $\gamma W^+ H^-$ and $Z W^+ H^-$ counterterms. The imaginary part of $\Sigma_{W^+H^+}(m_{H^\pm}^2)$ remains in diagrams 1 and 2 of Fig. 5, since it is not canceled by the $W^+ H^+$ mixing counterterm. This imaginary part also determines diagram 3 of Fig. 5 via Eq. 15.

We have checked explicitly that all the divergences in the 1PI diagrams that contribute to $e^+ e^- \rightarrow W^+ H^-$ are canceled by the counterterms.

IV. NUMERICAL RESULTS

In this section we examine the behavior of the cross section for $e^+ e^- \rightarrow W^+ H^-$ for various choices of SUSY parameters and evaluate the regions of parameter space in which the cross section is large enough to be observed for $m_{H^\pm} > \sqrt{s}/2$. As described in the Introduction, we assume data samples of 500 fb^{-1} at $\sqrt{s} = 500 \text{ GeV}$ and 1000 fb^{-1} at $\sqrt{s} = 1000 \text{ GeV}$. We choose an optimistic standard of detectability to be ten H^\pm production events in the LC data sample. Adding together the cross sections for $W^+ H^-$ and $W^- H^+$ production, our standard corresponds to a cross section for $W^+ H^-$ production of 0.01 fb at $\sqrt{s} = 500 \text{ GeV}$ and 0.005 fb at $\sqrt{s} = 1000 \text{ GeV}$. We assume that the e^+ beams are unpolarized. We compare the cross sections obtained with unpolarized e^- beams with those obtained with 80% left- or right-polarized e^- beams. We do not make any attempt to consider backgrounds or apply cuts; this is beyond the scope of our present analysis.

Unlike the case of the non-supersymmetric 2HDM, in which the top/bottom quark loops give by far the largest contribution to the cross section, in the full MSSM the fermionic loops involving charginos/neutralinos and the bosonic loops involving stops/sbottoms also give contributions of similar size. Although the stop/sbottom loops are enhanced by the large $H^- \tilde{t}_R \tilde{b}_L^*$ coupling (which is proportional to the top quark Yukawa coupling), these diagrams are suppressed by higher powers of the superparticle masses than the fermionic loops.

Diagram 1 in Fig. 2 and diagrams 1 and 3 in Fig. 4 decouple in the limit of heavy gauginos and Higgsinos, while diagrams 3-10 in Fig. 2 decouple in the limit of either

heavy sleptons or of heavy gauginos/Higgsinos. Squarks and sleptons contribute to diagram 2 in Fig. 2 and 2 and 4 in Fig. 4, where stops/sbottoms give the largest contribution because of the large top quark Yukawa coupling.

In our numerical analysis, we use a common sfermion mass scale $M_{\text{SUSY}} = 200 \text{ GeV}$ for all the squarks and sleptons. M_{SUSY} is the soft SUSY-breaking mass parameter that enters the diagonal elements of the squark and slepton mass matrices. We also include the additional D -term contributions to squark and slepton masses, which is crucial for the Slavnov-Taylor identity (Eq. 15) to hold. We study two different choices for the trilinear A couplings: (I) $A_t = A_b = 0$ and (II) $A_t = A_b = 200 \text{ GeV}$. Along with the μ parameter and $\tan \beta$, A_t determines the left-right mixing in the stop sector, which plays an important role for relatively light M_{SUSY} . In addition, the μ parameter determines the Higgsino masses. In most of our analysis we choose $\mu = 500 \text{ GeV}$; we also consider $\mu = 100 \text{ GeV}$ when examining the $\tan \beta$ dependence of the cross section. We fix the U(1) and SU(2) gaugino mass parameters to be $2M_1 = M_2 = 200 \text{ GeV}$. Working consistently at the one-loop level, we use the tree-level relations for the Higgs masses and mixing angles in terms of m_{A^0} and $\tan \beta$. We have verified numerically that using the radiatively corrected values for the CP-even Higgs masses and mixing angle does not change our numerical results in any significant way.

In what follows, we have taken all the SUSY breaking masses for the squarks and sleptons to be the same for simplicity. With M_{SUSY} as low as 200 GeV , the radiatively corrected mass of the lightest CP-even MSSM Higgs boson h^0 lies below the current experimental Higgs search bound. However, it is of course possible to choose M_{SUSY} for the stop/sbottom sector to be large and/or to impose large left-right mixing in the stop sector so that the mass of h^0 is increased above the experimental bound, while still keeping the sleptons and first two generations of squarks relatively light so that they give large contributions to the $e^+ e^- \rightarrow W^\pm H^\mp$ cross section. In this case, the numerical results presented below will of course change slightly, but the general conclusions from our analysis will remain true. A more detailed analysis of the constraints due to the h^0 mass bound will be presented elsewhere [56].

Figures 7 and 8 show the dependence of the $e^+ e^- \rightarrow W^+ H^-$ cross section on the charged Higgs mass for $\tan \beta = 2.5$ and 7, respectively. In both cases we plot cross sections for $\sqrt{s} = 500 \text{ GeV}$ (left) and $\sqrt{s} = 1000 \text{ GeV}$ (right). Solid lines are the contributions from the non-SUSY 2HDM with the Higgs sector constrained by the MSSM mass and coupling relations.¹² The dotted

¹² The pure 2HDM contributions to $e^+ e^- \rightarrow W^+ H^-$ have been studied in Refs. [46, 47]. Our numerical results for the 2HDM are in close agreement with those of Refs. [46, 47], after taking into account a factor of $1/4$ from the average over the initial $e^+ e^-$ polarizations that was omitted in Ref. [46] [37], and noting that

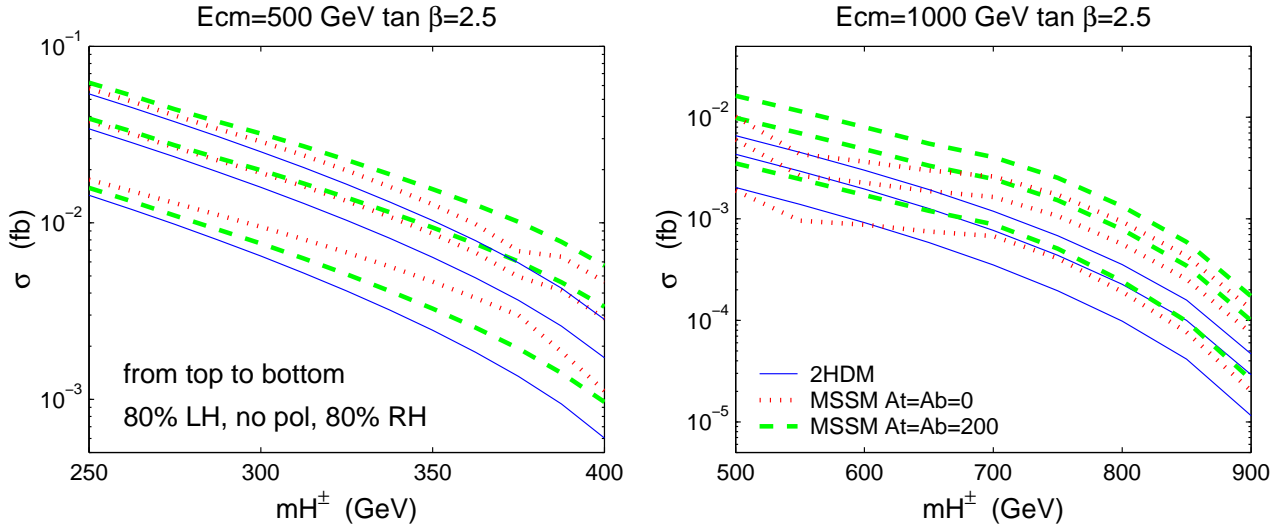


FIG. 7: The $e^+e^- \rightarrow W^+H^-$ cross section as a function of m_{H^\pm} for $\tan \beta = 2.5$, at $\sqrt{s} = 500$ GeV (left) and 1000 GeV (right). The trilinear couplings are chosen as $A_t = A_b = 0$ (dotted lines) and 200 GeV (dashed lines). The rest of the SUSY parameters are chosen to be $M_{\text{SUSY}} = 200$ GeV, $2M_1 = M_2 = 200$ GeV, and $\mu = 500$ GeV. The solid lines show the cross section in the non-SUSY 2HDM (with MSSM relations for the Higgs sector). In each plot, the lines from top to bottom are the cross sections for 80% left-polarized, unpolarized, and 80% right-polarized electrons.

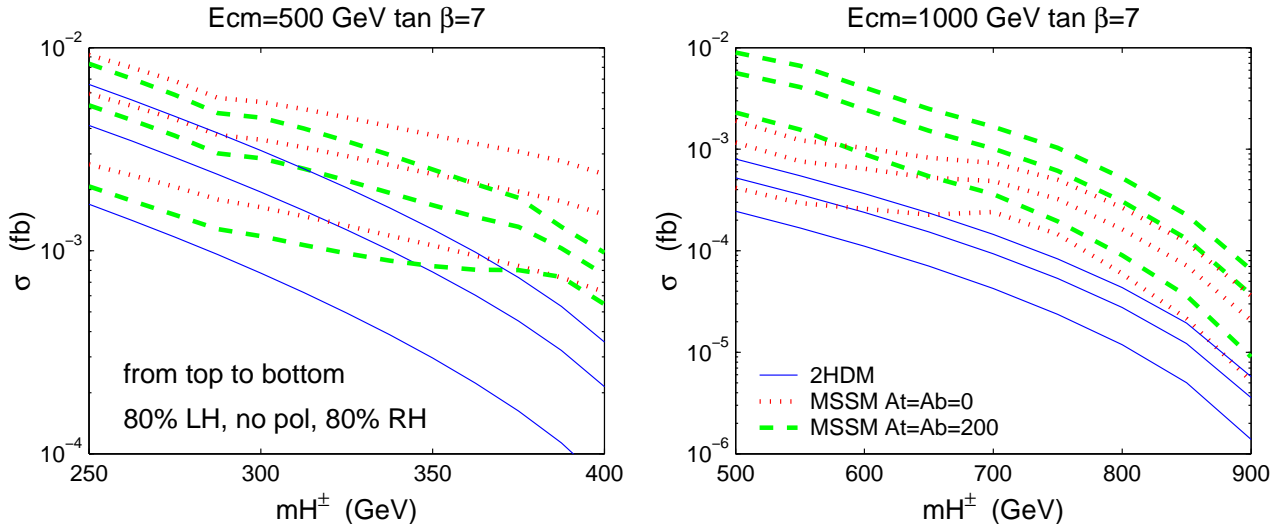


FIG. 8: The $e^+e^- \rightarrow W^+H^-$ cross section as a function of m_{H^\pm} for $\tan \beta = 7$. All other input parameters and notation are the same as in Fig. 7.

(dashed) lines show the cross sections in the full MSSM, including the contributions from all the superparticles, for $A_t = A_b = 0$ ($A_t = A_b = 200$ GeV). We compare the cross sections with 80% left-handed e^- polarization, no polarization, and 80% right-handed e^- polarization, which are denoted in each plot by the same type of lines,

from top to bottom. Left-handed e^- polarization always gives a larger cross section. The additional SUSY contributions generally enhance the cross section. In certain cases, for example $\sqrt{s}=1000$ GeV and $\tan \beta = 7$ (Fig. 8), the SUSY contributions increase the cross section by almost an order of magnitude. The cross sections decline as m_{H^\pm} increases; however, reasonable cross sections can be obtained for $m_{H^\pm} > \sqrt{s}/2$, especially for small $\tan \beta$.

The ten-event discovery reach in m_{H^\pm} is shown in Table I for a 500 GeV LC (requiring a cross section of 0.01 fb) and a 1000 GeV LC (requiring a cross section of 0.005

the results in Ref. [47] are the average over the spin states $e_L^+e_R^-$ and $e_R^+e_L^-$; for unpolarized beams the cross sections in Ref. [47] should be divided by two.

TABLE I: Ten-event discovery reach in m_{H^\pm} (in GeV) at a LC with an 80% left-polarized electron beam, for $\sqrt{s} = 500$ GeV ($\mathcal{L} = 500 \text{ fb}^{-1}$) and 1000 GeV ($\mathcal{L} = 1000 \text{ fb}^{-1}$). The corresponding reach with an unpolarized electron beam is given in parentheses. The SUSY parameters are as specified in the caption of Fig. 7.

\sqrt{s}	$\tan \beta = 2.5$		$\tan \beta = 7$	
	500 GeV	1000 GeV	500 GeV	1000 GeV
2HDM	352 (327)	535 (<500)	< 250	< 500
MSSM, $A_t = A_b = 0$	362 (344)	540 (512)	< 250	< 500
MSSM, $A_t = A_b = 200$ GeV	375 (347)	667 (600)	< 250	581 (517)

fb). Using an 80% left-polarized electron beam generally increases the reach by at least 20 GeV compared to the unpolarized case. The increase in the reach in the MSSM compared to the 2HDM is larger at larger $\tan \beta$ or higher LC center-of-mass energy. In the following discussion, we will consider the results for an 80% left-polarized electron beam. For $\tan \beta = 2.5$, a charged Higgs with mass up to 375 GeV (667 GeV) could be detected at a 500 GeV (1000 GeV) LC. For favorable SUSY parameters, the SUSY contributions can increase the reach by about 20 GeV at $\sqrt{s} = 500$ GeV and by more than 100 GeV at $\sqrt{s} = 1000$ GeV, compared to the non-SUSY 2HDM. At $\tan \beta = 7$, the cross section is generally too small to be observed at the ten-event level; however, a reach in m_{H^\pm} up to about 580 GeV is still possible at a 1000 GeV machine. The dependence of the cross section on A_t for low $M_{\text{SUSY}} = 200$ GeV is due to the effects of left-right mixing in the stop sector. For larger values of M_{SUSY} , the squark contributions become less important and the dependence on A_t becomes much less significant. The cross section is also sensitive to the value of the μ parameter. For example, lowering μ to 100 GeV increases the ten-event discovery reach in m_{H^\pm} to 390 GeV at $\tan \beta = 2.5$ or 300 GeV for $\tan \beta = 7$ at a 500 GeV LC, almost independent of A_t (see Fig. 9).

Figure 9 shows the $\tan \beta$ dependence of the $e^+e^- \rightarrow W^\pm H^\mp$ cross section for 80% left-polarized electrons. We plot two different values for μ , 100 and 500 GeV, to show the μ dependence as well as the dependence on A_t for small $M_{\text{SUSY}} = 200$ GeV. For $\mu = 500$ GeV, values of $\tan \beta$ above 20 lead to a negative mass-squared for the lighter sbottom and are forbidden. From Fig. 9 we can see that while the cross section in the 2HDM (solid line) falls rapidly with increasing $\tan \beta$, the cross section in the MSSM experiences a much milder drop as $\tan \beta$ increases. Thus the reach in $\tan \beta$ in the MSSM is larger than in the 2HDM. At a 500 GeV machine, for $m_{H^\pm} = 350$ GeV, the ten-event discovery reach is $\tan \beta \leq 5.8$ in the MSSM with favorable parameters as shown in Fig. 9, compared to $\tan \beta < 2.5$ in the 2HDM. At a 1000 GeV machine, for $m_{H^\pm} = 600$ GeV, the ten-event discovery reach is $\tan \beta \lesssim 5$ in the MSSM, while in the 2HDM even $\tan \beta \sim 2$ is not detectable. In Table II we show the maximum ten-event discovery reach in $\tan \beta$ when m_{H^\pm} is just above $\sqrt{s}/2$. For a 500 GeV machine, we find that a reach up to $\tan \beta \lesssim 9$ is possible for $m_{H^\pm} \simeq 250$ GeV. For a 1000 GeV machine, while in most cases we find a reach up to

$\tan \beta \lesssim 5$ for $m_{H^\pm} \simeq 500$ GeV, in certain cases a wide range of $\tan \beta$ values can be explored.

For the relatively low values of M_{SUSY} , M_1 and M_2 used in our analysis, the dependence on μ is complicated. We find an enhancement of the cross section over the 2HDM for most values of μ . However, there are values of μ that lead to a large suppression in the cross section. For example, at $\sqrt{s} = 500$ GeV with a left-polarized electron beam, $m_{H^\pm} = 350$ GeV, $\tan \beta = 2.5$, $A_t = A_b = 200$ GeV, and μ around 800 GeV, there is a large cancellation between the 2HDM and SUSY matrix elements, leading to a suppression of the cross section. Furthermore, changing the relative signs of M_1 , M_2 and μ can alter the SUSY contribution to the cross section.

V. CONCLUSIONS

We studied the single charged Higgs production process $e^+e^- \rightarrow W^\pm H^\mp$ at a 500 GeV and a 1000 GeV linear collider, including the complete MSSM contributions at one loop. At small $\tan \beta$, the reach in m_{H^\pm} from this process extends above the kinematic threshold ($m_{H^\pm} \simeq \sqrt{s}/2$) for $e^+e^- \rightarrow H^+H^-$ pair production. We found that light SUSY particles with masses of order 200 GeV enhance the cross section in most of the parameter space. At small $\tan \beta$, an increase in the reach in m_{H^\pm} by about 20 GeV in the full MSSM compared to that in the 2HDM is possible at a 500 GeV machine, and by more than 100 GeV at a 1000 GeV machine. In particular, with favorable SUSY parameters and $\tan \beta = 2.5$, this process yields more than 10 $W^\pm H^\mp$ events for $m_{H^\pm} \lesssim 350$ GeV in 500 fb^{-1} at a 500 GeV collider, or $m_{H^\pm} \lesssim 600$ GeV in 1000 fb^{-1} at a 1000 GeV collider, assuming unpolarized beams. At large $\tan \beta$, an order of magnitude enhancement of the cross section compared to the 2HDM is possible, so that the cross section suffers only a moderate decrease with increasing $\tan \beta$. The reach in $\tan \beta$ is therefore enhanced; with favorable SUSY parameters and $m_{H^\pm} \simeq \sqrt{s}/2$, this process yields more than 10 $W^\pm H^\mp$ events for $\tan \beta \lesssim 6$ at a 500 GeV collider. We also found that an 80% left-polarized electron beam enhances the cross section by about 50% and improves the discovery reach by at least an additional 25 GeV; in particular, the reach at $\tan \beta = 2.5$ improves to $m_{H^\pm} \lesssim 375$ GeV at a 500 GeV collider, or $m_{H^\pm} \lesssim 670$ GeV at a 1000 GeV collider, and the reach in $\tan \beta$ improves to ~ 8.5 at a

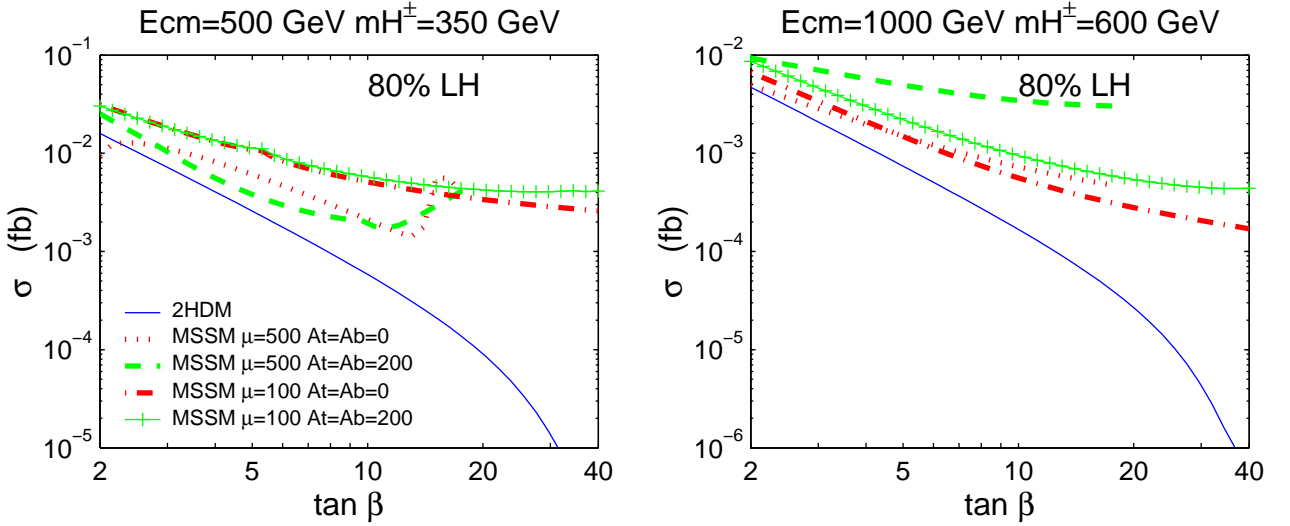


FIG. 9: The $e^+e^- \rightarrow W^+H^-$ cross section as a function of $\tan\beta$ for 80% left-polarized electrons, with $\sqrt{s} = 500$ GeV, $m_{H^\pm} = 350$ GeV (left) and $\sqrt{s} = 1000$ GeV, $m_{H^\pm} = 600$ GeV (right). Four different choices for μ and $A_t = A_b$ are shown: $\mu = 500$ GeV, $A_t = A_b = 0$ (dotted line); $\mu = 500$ GeV, $A_t = A_b = 200$ GeV (dashed line); $\mu = 100$ GeV, $A_t = A_b = 0$ (dash-dotted line); and $\mu = 100$ GeV, $A_t = A_b = 200$ GeV (“+” line). The remaining SUSY parameters are $M_{\text{SUSY}} = 200$ GeV and $2M_1 = M_2 = 200$ GeV. The solid lines show the cross section in the non-SUSY 2HDM (with MSSM relations for the Higgs sector).

TABLE II: Ten-event discovery reach in $\tan\beta$ for $m_{H^\pm} \simeq \sqrt{s}/2$ at a LC with an 80% left-polarized electron beam, for $\sqrt{s} = 500$ GeV ($\mathcal{L} = 500 \text{ fb}^{-1}$) and 1000 GeV ($\mathcal{L} = 1000 \text{ fb}^{-1}$). The corresponding reach with an unpolarized electron beam is given in parentheses. The SUSY parameters are as specified in the caption of Fig. 9.

\sqrt{s}	500 GeV		1000 GeV		
	μ	100 GeV	500 GeV	100 GeV	500 GeV
2HDM		5.8 (4.6)		2.9 (2.3)	
MSSM, $A_t = A_b = 0$		8.6 (5.6)	6.7 (5.4)	3.8 (2.9)	3.5 (2.8)
MSSM, $A_t = A_b = 200$ GeV		8.7 (5.9)	6.4 (4.9)	4.7 (3.4)	~ 20

500 GeV collider.

The process $e^+e^- \rightarrow W^+H^-$ in the MSSM with light superpartners is very promising compared to the other single charged Higgs boson production modes that have been considered to date. At the e^+e^- collider, the processes $e^+e^- \rightarrow \tau^-\bar{\nu}H^+$ and $t\bar{b}H^+$ are complementary to W^+H^- production in that their cross sections are largest at high values of $\tan\beta$. For $\tan\beta \simeq 40$, they provide a reach of $m_{H^\pm} \lesssim 275$ GeV and 260 GeV, respectively, at a 500 GeV collider, and $m_{H^\pm} \lesssim 520$ GeV and 560 GeV, respectively, at a 1000 GeV collider. If 1000 fb^{-1} of e^+e^- luminosity at 1000 GeV is devoted to $\gamma\gamma$ collisions, the reach in $\tau^-\bar{\nu}H^+$ production can be extended to $m_{H^\pm} \lesssim 700$ GeV at high $\tan\beta \gtrsim 30$. At an $e^-\gamma$ collider, the cross section for νH^- production in the 2HDM is too small to be seen in the typical integrated luminosity of 100 fb^{-1} in the high-energy part of the γ spectrum. This process could become promising in the MSSM if its cross section is enhanced by the contributions of light superpartners, or if the $e^-\gamma$ luminosity is increased. Finally, if 1000 fb^{-1} of e^+e^- luminosity at 1000 GeV is devoted

to $\gamma\gamma$ collisions, the process $\gamma\gamma \rightarrow W^+H^-$ in the MSSM will be competitive to $e^+e^- \rightarrow W^+H^-$. For light superparticles, this process provides a reach in m_{H^\pm} above 600 GeV for $\tan\beta = 2$ and $m_{H^\pm} \lesssim 520$ GeV for $\tan\beta = 6$.

A few additional processes that have not yet been computed may be promising for single heavy Higgs boson production at an e^+e^- collider. The behavior of the SM Higgs production cross sections leads us to expect that weak boson fusion processes will naturally have larger cross sections than Higgsstrahlung-type processes at $\sqrt{s} \sim 1000$ GeV. The process $e^+e^- \rightarrow \bar{\nu}e^-H^+$ may thus be promising. The calculation of this process in the 2HDM will be quite straightforward since the only contributions come from the loop-induced ZW^+H^- and γW^+H^- vertices [56]. The process $e^+e^- \rightarrow \nu\bar{\nu}A^0$ may also be promising. Preliminary results for the top/bottom quark loop contributions in the 2HDM indicate, however, that this process is too small to be observed for $m_{A^0} > \sqrt{s}/2$ [39]. This process could become observable if the addition of the full 2HDM and MSSM contributions enhances the cross section sufficiently [57].

Acknowledgments

We are grateful to Abdesslam Arhrib, David Asner, Marcela Carena, Tom Farris, Jack Gunion, Howie Haber, Sven Heinemeyer, Uli Nierste, Michel Capdequi-Peyranère, Tilman Plehn and Dave Rainwater for helpful conversations. We also thank the Aspen Center for Physics, where this project was begun. HEL thanks the Physics Department at CalTech for their hospitality during part of this work. Fermilab is operated by Universities Research Association Inc. under contract no. DE-AC02-76CH03000 with the U.S. Department of Energy. S.S. is supported by the DOE under grant DE-FG03-92-ER-40701 and by the John A. McCone Fellowship.

APPENDIX A: NOTATION AND CONVENTIONS

For couplings and Feynman rules we follow the conventions of Ref. [58]. We follow the notation of Ref. [46] for the one-loop integrals. The one-point integral is:

$$\frac{i}{16\pi^2} A(m^2) = \int \frac{d^D q}{(2\pi)^D} \frac{1}{(q^2 - m^2)}, \quad (\text{A1})$$

where D is the number of dimensions. The two-point integrals are:

$$\frac{i}{16\pi^2} \{B_0, k^\mu B_1\} (k^2, m_0^2, m_1^2) = \quad (\text{A2})$$

The three-point integrals are:

$$\begin{aligned} \frac{i}{16\pi^2} \{C_0, C^\mu, C^{\mu\nu}\} &= \\ \int \frac{d^D q}{(2\pi)^D} \frac{\{1, q^\mu, q^\mu q^\nu\}}{(q^2 - m_0^2)((q + k_1)^2 - m_1^2)((q + k_2)^2 - m_2^2)}, \end{aligned} \quad (\text{A3})$$

where the tensor integrals are decomposed in terms of scalar components as

$$\begin{aligned} C^\mu &= k_1^\mu C_1 + k_2^\mu C_2 \\ C^{\mu\nu} &= g^{\mu\nu} C_{00} + k_1^\mu k_1^\nu C_{11} + k_2^\mu k_2^\nu C_{22} \\ &\quad + (k_1^\mu k_2^\nu + k_2^\mu k_1^\nu) C_{12}. \end{aligned} \quad (\text{A4})$$

The arguments of the scalar three-point integrals are $(k_1^2, (k_2 - k_1)^2, k_2^2, m_0^2, m_1^2, m_2^2)$. The four-point integrals are:

$$\frac{i}{16\pi^2} \{D_0, D^\mu, D^{\mu\nu}\} = \int \frac{d^D q}{(2\pi)^D} \frac{\{1, q^\mu, q^\mu q^\nu\}}{(q^2 - m_0^2)((q + k_1)^2 - m_1^2)((q + k_2)^2 - m_2^2)((q + k_3)^2 - m_3^2)}, \quad (\text{A5})$$

where the tensor integrals are decomposed in terms of scalar components as

$$\begin{aligned} D^\mu &= k_1^\mu D_1 + k_2^\mu D_2 + k_3^\mu D_3 \\ D^{\mu\nu} &= g^{\mu\nu} D_{00} + k_1^\mu k_1^\nu D_{11} + k_2^\mu k_2^\nu D_{22} + k_3^\mu k_3^\nu D_{33} \\ &\quad + (k_1^\mu k_2^\nu + k_2^\mu k_1^\nu) D_{12} + (k_1^\mu k_3^\nu + k_3^\mu k_1^\nu) D_{13} \\ &\quad + (k_2^\mu k_3^\nu + k_3^\mu k_2^\nu) D_{23}. \end{aligned} \quad (\text{A6})$$

The arguments of the scalar four-point integrals are $(k_1^2, (k_2 - k_1)^2, (k_3 - k_2)^2, k_3^2, k_2^2, (k_1 - k_3)^2, m_0^2, m_1^2, m_2^2, m_3^2)$.

APPENDIX B: 2HDM CONTRIBUTIONS

Explicit results for the matrix elements for $e^+ e^- \rightarrow W^+ H^-$ in the 2HDM were given in Ref. [46]. We have calculated all the 2HDM diagrams independently and give the formulae here for completeness. After correcting a few typographical errors [37] in the formulae of

Ref. [46], we find agreement with all of their results except for Figs. 5.2 and 5.3, which differ by an overall sign.

The quark triangles that appear in Figs. 1.1 and 1.2 were also computed in Ref. [40] and agree with our results. (Note that Ref. [40] uses the convention $\varepsilon_{0123} = 1$, which is opposite to our convention.)

For convenience, we list here our notation for the gauge and Yukawa coupling coefficients used in this section.

The photon coupling coefficients to leptons/quarks are:

$$g_\gamma^{fL} = g_\gamma^{fR} = -e_f, \quad (\text{B1})$$

where the electric charges are $e_\nu = 0$, $e_e = -1$, $e_u = 2/3$, and $e_d = -1/3$.

The Z boson coupling coefficients to leptons/quarks are:

$$g_Z^{fL} = (-T_3 + e_f s_W^2)/s_W c_W, \quad g_Z^{fR} = (e_f s_W^2)/s_W c_W, \quad (\text{B2})$$

where $T_3 = 1/2$ for ν , u and $T_3 = -1/2$ for e , d .

For the W boson coupling to leptons/quarks we define:

$$g_W = -1/\sqrt{2}s_W. \quad (B3)$$

The H^\pm and G^\pm coupling coefficients to top/bottom quarks are (the couplings to leptons and first and second generation quarks are small and taken to be zero):

y_{Htb}^L	y_{Htb}^R	y_{Gtb}^L	y_{Gtb}^R
$m_t \cot \beta / \sqrt{2} m_W s_W$	$m_b \tan \beta / \sqrt{2} m_W s_W$	$-m_b / \sqrt{2} m_W s_W$	$m_t / \sqrt{2} m_W s_W$

The coefficients for couplings of three Higgs bosons are:

$g_{H^- AG^+}$	$-im_W/2s_W$
$g_{H^- h^0 H^+}$	$-m_W s_{\beta\alpha}/s_W - m_Z \cos 2\beta \sin(\beta + \alpha)/2s_W c_W$
$g_{H^- H^0 H^+}$	$-m_W c_{\beta\alpha}/s_W + m_Z \cos 2\beta \cos(\beta + \alpha)/2s_W c_W$
$g_{H^- h^0 G^+}$	$m_W c_{\beta\alpha}/2s_W - m_Z \sin 2\beta \sin(\beta + \alpha)/2s_W c_W$
$g_{H^- H^0 G^+}$	$-m_W s_{\beta\alpha}/2s_W + m_Z \sin 2\beta \cos(\beta + \alpha)/2s_W c_W$
$g_{G^- h^0 G^+}$	$m_Z \cos 2\beta \sin(\beta + \alpha)/2s_W c_W$
$g_{G^- H^0 G^+}$	$-m_Z \cos 2\beta \cos(\beta + \alpha)/2s_W c_W$

where $s_{\beta\alpha} = \sin(\beta - \alpha)$ and $c_{\beta\alpha} = \cos(\beta - \alpha)$.

We now list our results for the 2HDM diagrams.

Fig. 1.1:

$$\begin{aligned} \mathcal{M} = \frac{2\alpha^2 N_c g_W}{s - m_V^2} & \{ [- (m_t g_V^{dL} y_{Htb}^L + m_b (g_V^{dL} - g_V^{dR}) y_{Htb}^R) B_0 + 2g_V^{dL} (m_t y_{Htb}^L + m_b y_{Htb}^R) C_{00} \\ & + (-g_V^{dL} (m_t y_{Htb}^L + m_b y_{Htb}^R) m_W^2 + (m_t g_V^{dL} y_{Htb}^L - m_b g_V^{dR} y_{Htb}^R) k_1 \cdot k_2) C_1 \\ & + (g_V^{dL} (m_t y_{Htb}^L + m_b y_{Htb}^R) k_1 \cdot k_2 - (m_t g_V^{dL} y_{Htb}^L - m_b g_V^{dR} y_{Htb}^R) m_{H^\pm}^2) C_2 \\ & + (-m_t^3 g_V^{dL} y_{Htb}^L - m_t^2 m_b (g_V^{dL} - g_V^{dR}) y_{Htb}^R + m_t m_b^2 g_V^{dR} y_{Htb}^L + m_t g_V^{dL} y_{Htb}^L k_1 \cdot k_2) C_0] [g_V^{eR} \mathcal{A}_1 + g_V^{eL} \mathcal{A}_2] \\ & + [-2g_V^{dL} (m_t y_{Htb}^L + m_b y_{Htb}^R) (C_{12} + C_{22}) - g_V^{dL} (3m_t y_{Htb}^L + m_b y_{Htb}^R) C_2 - (m_t g_V^{dL} y_{Htb}^L - m_b g_V^{dR} y_{Htb}^R) C_1 \\ & - m_t g_V^{dL} y_{Htb}^L C_0] [g_V^{eR} (\mathcal{A}_3 + \mathcal{A}_5) + g_V^{eL} (\mathcal{A}_4 + \mathcal{A}_6)] \\ & + [m_t g_V^{dL} y_{Htb}^L C_0 + (m_t g_V^{dL} y_{Htb}^L + m_b g_V^{dR} y_{Htb}^R) C_1 + g_V^{dL} (m_t y_{Htb}^L + m_b y_{Htb}^R) C_2] (g_V^{eR} \mathcal{A}_7 + g_V^{eL} \mathcal{A}_8) \} , \end{aligned} \quad (B4)$$

with the arguments for the integral functions as $B(s, m_b^2, m_b^2)$, $C(m_W^2, s, m_{H^\pm}^2, m_t^2, m_b^2, m_b^2)$.

Fig. 1.2: Similar to Fig. 1.1 with the exchange of

$$m_t \leftrightarrow m_b, \quad g_V^{dL} \leftrightarrow g_V^{uL}, \quad g_V^{dR} \leftrightarrow g_V^{uR}, \quad y_{Htb}^L \leftrightarrow y_{Htb}^R; \quad \mathcal{A}_7, \mathcal{A}_8 \text{ terms flip sign.} \quad (B5)$$

Fig. 1.3:

$$\begin{aligned} \mathcal{M} = \frac{\alpha^2}{s - m_V^2} & g_{VWW} g_{WWSGHWS} \\ & [-B_0 - (s + m_S^2 - m_W^2) C_0 - (s + m_W^2 - m_{H^\pm}^2) C_1 + (s - m_W^2 + m_{H^\pm}^2) C_2 + C_{00}] (g_V^{eR} \mathcal{A}_1 + g_V^{eL} \mathcal{A}_2) \\ & + (4C_1 + C_2 - C_{12} - C_{22}) [g_V^{eR} (\mathcal{A}_3 + \mathcal{A}_5) + g_V^{eL} (\mathcal{A}_4 + \mathcal{A}_6)] , \end{aligned} \quad (B6)$$

with the arguments for the integral functions as $B(s, m_W^2, m_W^2)$, $C(m_W^2, s, m_{H^\pm}^2, m_S^2, m_W^2, m_W^2)$. The couplings are given in the following table:

S	$g_{\gamma WW}$	g_{ZWW}	g_{HWS}	g_{WWS}
h^0	-1	$-c_W/s_W$	$c_{\beta\alpha}/2s_W$	$m_W s_{\beta\alpha}/s_W$
H^0	-1	$-c_W/s_W$	$-s_{\beta\alpha}/2s_W$	$m_W c_{\beta\alpha}/s_W$

Fig. 1.4:

$$\begin{aligned} \mathcal{M} = \frac{2\alpha^2}{s - m_Z^2} & g_{ZS_i S_j} g_{HWS_i} g_{WWS_j} \{ C_{00} (g_V^{eR} \mathcal{A}_1 + g_V^{eL} \mathcal{A}_2) \\ & - (2C_0 + 2C_1 + 3C_2 + C_{12} + C_{22}) [g_V^{eR} (\mathcal{A}_3 + \mathcal{A}_5) + g_V^{eL} (\mathcal{A}_4 + \mathcal{A}_6)] \} , \end{aligned} \quad (B7)$$

with the arguments for the integral functions as $C(m_W^2, s, m_{H^\pm}^2, m_W^2, m_{S_i}^2, m_{S_j}^2)$. The couplings are given in the following table:

S_i	S_j	$g_{ZS_iS_j}$	g_{HWS_i}	g_{WWS_j}
A^0	h^0	$-ic_{\beta\alpha}/2s_W c_W$	$-i/2s_W$	$m_W s_{\beta\alpha}/s_W$
A^0	H^0	$is_{\beta\alpha}/2s_W c_W$	$-i/2s_W$	$m_W c_{\beta\alpha}/s_W$

Fig. 1.5:

$$\begin{aligned} \mathcal{M} = & -\frac{4\alpha^2}{s - m_V^2} g_{V S_i S_j} g_{H S_i S_k} g_{W S_j S_k} \{ C_{00} (g_V^{eR} \mathcal{A}_1 + g_V^{eL} \mathcal{A}_2) \\ & - (C_2 + C_{12} + C_{22}) [g_V^{eR} (\mathcal{A}_3 + \mathcal{A}_5) + g_V^{eL} (\mathcal{A}_4 + \mathcal{A}_6)] \}, \end{aligned} \quad (B8)$$

with the arguments for the integral functions as $C(m_W^2, s, m_{H^\pm}^2, m_{S_k}^2, m_{S_j}^2, m_{S_i}^2)$. The couplings are given in the following table:

S_i	S_j	S_k	$g_{\gamma S_i S_j}$	$g_{Z S_i S_j}$	$g_{H S_i S_k}$	$g_{W S_j S_k}$
A^0	h^0	G^\pm	0	$-ic_{\beta\alpha}/2s_W c_W$	$g_{H^- A G^+}$	$-s_{\beta\alpha}/2s_W$
A^0	H^0	G^\pm	0	$is_{\beta\alpha}/2s_W c_W$	$g_{H^- A G^+}$	$-c_{\beta\alpha}/2s_W$
h^0	A^0	H^\pm	0	$ic_{\beta\alpha}/2s_W c_W$	$g_{H^- h^0 H^+}$	$i/2s_W$
H^0	A^0	H^\pm	0	$-is_{\beta\alpha}/2s_W c_W$	$g_{H^- H^0 H^+}$	$i/2s_W$
h^0	G^0	G^\pm	0	$is_{\beta\alpha}/2s_W c_W$	$g_{H^- h^0 G^+}$	$i/2s_W$
H^0	G^0	G^\pm	0	$ic_{\beta\alpha}/2s_W c_W$	$g_{H^- H^0 G^+}$	$i/2s_W$
G^\pm	G^\pm	h^0	1	$\cos(2\theta_W)/2s_W c_W$	$g_{H^- h^0 G^+}$	$s_{\beta\alpha}/2s_W$
G^\pm	G^\pm	H^0	1	$\cos(2\theta_W)/2s_W c_W$	$g_{H^- H^0 G^+}$	$c_{\beta\alpha}/2s_W$
H^\pm	H^\pm	h^0	1	$\cos(2\theta_W)/2s_W c_W$	$g_{H^- h^0 H^+}$	$c_{\beta\alpha}/2s_W$
H^\pm	H^\pm	H^0	1	$\cos(2\theta_W)/2s_W c_W$	$g_{H^- H^0 H^+}$	$-s_{\beta\alpha}/2s_W$

Fig. 1.6:

$$\mathcal{M} = \frac{\alpha^2}{s - m_V^2} g_{V V' S_i} g_{W V' S_j} g_{H S_i S_j} C_0 (g_V^{eR} \mathcal{A}_1 + g_V^{eL} \mathcal{A}_2), \quad (B9)$$

with the arguments for the integral functions as $C(m_W^2, s, m_{H^\pm}^2, m_{S_j}^2, m_{V'}^2, m_{S_i}^2)$. The couplings are given in the following table:

S_i	S_j	V'	$g_{\gamma V' S_i}$	$g_{Z V' S_i}$	$g_{H S_i S_j}$	$g_{W V' S_j}$
h^0	G^\pm	Z	0	$m_Z s_{\beta\alpha}/s_W c_W$	$g_{H^- h^0 G^+}$	$-m_Z s_W$
H^0	G^\pm	Z	0	$m_Z c_{\beta\alpha}/s_W c_W$	$g_{H^- H^0 G^+}$	$-m_Z s_W$
G^\pm	h^0	W^\pm	m_W	$-m_Z s_W$	$g_{H^- h^0 G^+}$	$m_W s_{\beta\alpha}/s_W$
G^\pm	H^0	W^\pm	m_W	$-m_Z s_W$	$g_{H^- H^0 G^+}$	$m_W c_{\beta\alpha}/s_W$

Fig. 1.7:

$$\begin{aligned} \mathcal{M} = & \frac{2\alpha^2}{s - m_V^2} g_{V V' S_i} g_{H V' S_j} g_{W S_i S_j} \{ -C_{00} (g_V^{eR} \mathcal{A}_1 + g_V^{eL} \mathcal{A}_2) \\ & + (-C_2 + C_{12} + C_{22}) [g_V^{eR} (\mathcal{A}_3 + \mathcal{A}_5) + g_V^{eL} (\mathcal{A}_4 + \mathcal{A}_6)] \}, \end{aligned} \quad (B10)$$

with the arguments for the integral functions as $C(m_W^2, s, m_{H^\pm}^2, m_{S_j}^2, m_{S_i}^2, m_{V'}^2)$. The couplings are given in the following table:

S_i	S_j	V'	$g_{\gamma V' S_i}$	$g_{Z V' S_i}$	$g_{H V' S_j}$	$g_{W S_i S_j}$
h^0	H^\pm	Z	0	$m_Z s_{\beta\alpha}/s_W c_W$	$\cos(2\theta_W)/2s_W c_W$	$-c_{\beta\alpha}/2s_W$
H^0	H^\pm	Z	0	$m_Z c_{\beta\alpha}/s_W c_W$	$\cos(2\theta_W)/2s_W c_W$	$s_{\beta\alpha}/2s_W$
G^\pm	h^0	W^\pm	m_W	$-m_Z s_W$	$c_{\beta\alpha}/2s_W$	$s_{\beta\alpha}/2s_W$
G^\pm	H^0	W^\pm	m_W	$-m_Z s_W$	$-s_{\beta\alpha}/2s_W$	$c_{\beta\alpha}/2s_W$

Fig. 1.8:

$$\mathcal{M} = \frac{\alpha^2}{s - m_Z^2} g_{ZZS} g_{HWS} g_{ZWW} \left\{ \left[B_0 + (2m_{H^\pm}^2 + 3m_W^2 - 2s)C_0 - (s - m_{H^\pm}^2 - 3m_W^2)C_1 - (s - m_W^2 - 3m_{H^\pm}^2)C_2 - C_{00} \right] (g_V^{eR} \mathcal{A}_1 + g_V^{eL} \mathcal{A}_2) \right. \\ \left. + (2C_0 - 2C_1 + 3C_2 + C_{12} + C_{22}) [g_V^{eR} (\mathcal{A}_3 + \mathcal{A}_5) + g_V^{eL} (\mathcal{A}_4 + \mathcal{A}_6)] \right\}, \quad (B11)$$

with the arguments for the integral functions as $B(s, m_Z^2, m_S^2)$, $C(m_W^2, s, m_{H^\pm}^2, m_W^2, m_Z^2, m_S^2)$. The couplings are given in the following table:

S	g_{ZZS}	g_{HWS}	g_{ZWW}
h^0	$m_Z s_{\beta\alpha} / s_W c_W$	$c_{\beta\alpha} / 2s_W$	$-c_W / s_W$
H^0	$m_Z c_{\beta\alpha} / s_W c_W$	$-s_{\beta\alpha} / 2s_W$	$-c_W / s_W$

Fig. 1.9:

$$\mathcal{M} = -\frac{\alpha^2 g_{VWHS} g_{WWS}}{s - m_V^2} B_0 (g_V^{eR} \mathcal{A}_1 + g_V^{eL} \mathcal{A}_2) \quad (B12)$$

with the arguments for the integral functions as $B(m_W^2, m_S^2, m_W^2)$. The couplings are given in the following table:

S	$g_{\gamma HWS}$	g_{ZHWS}	g_{WWS}
h^0	$c_{\beta\alpha} / 2s_W$	$-c_{\beta\alpha} / 2c_W$	$m_W s_{\beta\alpha} / s_W$
H^0	$-s_{\beta\alpha} / 2s_W$	$s_{\beta\alpha} / 2c_W$	$m_W c_{\beta\alpha} / s_W$

Fig. 1.10:

$$\mathcal{M} = \frac{\alpha^2 g_{VWS_i S_j} g_{HS_i S_j}}{s - m_V^2} B_0 (g_V^{eR} \mathcal{A}_1 + g_V^{eL} \mathcal{A}_2) \quad (B13)$$

Fig. 1.12:

$$\mathcal{M} = \alpha^2 g_W^2 g_{WWS} g_{HWS} \left\{ [C_0 + (m_S^2 - u)D_0 + (m_W^2 - u)D_1 + (u - m_{H^\pm}^2)D_3] \mathcal{A}_2 - 4D_1 \mathcal{A}_6 \right\}, \quad (B15)$$

with the arguments for the integrals as $C(m_e^2, m_e^2, s, m_W^2, 0, m_W^2)$, $D(m_W^2, m_e^2, m_e^2, m_{H^\pm}^2, u, s, m_S^2, m_W^2, 0, m_W^2)$. The couplings are given in the following table:

S	g_{WWS}	g_{HWS}
h^0	$m_W s_{\beta\alpha} / s_W$	$c_{\beta\alpha} / 2s_W$
H^0	$m_W c_{\beta\alpha} / s_W$	$-s_{\beta\alpha} / 2s_W$

Fig. 3.1:

$$\Sigma_{W+H^+}^f(k^2) = \frac{N_c \alpha}{2\pi} g_W \left[(m_t y_{Htb}^L + m_b y_{Htb}^R) B_1 + m_b y_{Htb}^R B_0 \right], \quad (B16)$$

with the arguments for the integral functions as $B(k^2, m_b^2, m_t^2)$, for k being the external momentum.

Fig. 3.2 + 3.3:

$$\Sigma_{W+H^+}^b(k^2) = \frac{\alpha}{8\pi s_W^2} \left[c_{\beta\alpha} s_W g_{H-h^0 H^+} (2B_1(k^2, m_{h^0}^2, m_{H^\pm}^2) + B_0(k^2, m_{h^0}^2, m_{H^\pm}^2)) \right. \\ \left. - s_{\beta\alpha} s_W g_{H-H^0 H^+} (2B_1(k^2, m_{h^0}^2, m_{H^\pm}^2) + B_0(k^2, m_{h^0}^2, m_{H^\pm}^2)) \right. \\ \left. + s_{\beta\alpha} s_W g_{H-h^0 G^+} (2B_1(k^2, m_{h^0}^2, m_W^2) + B_0(k^2, m_{h^0}^2, m_W^2)) \right]$$

with the arguments for the integral functions as $B(m_{H^\pm}^2, m_{S_j}^2, m_{S_i}^2)$. The couplings are given in the following table:

S_i	S_j	$g_{\gamma W S_i S_j}$	$g_{ZWS_i S_j}$	$g_{HS_i S_j}$
h^0	H^\pm	$c_{\beta\alpha} / 2s_W$	$-c_{\beta\alpha} / 2c_W$	$g_{H-h^0 H^+}$
H^0	H^\pm	$-s_{\beta\alpha} / 2s_W$	$s_{\beta\alpha} / 2c_W$	$g_{H-H^0 H^+}$
h^0	G^\pm	$s_{\beta\alpha} / 2s_W$	$-s_{\beta\alpha} / 2c_W$	$g_{H-h^0 G^+}$
H^0	G^\pm	$c_{\beta\alpha} / 2s_W$	$-c_{\beta\alpha} / 2c_W$	$g_{H-H^0 G^+}$

Fig. 1.11:

$$\mathcal{M} = -\frac{\alpha^2 g_{ZHWS} g_{ZZS}}{s - m_Z^2} B_0 (g_V^{eR} \mathcal{A}_1 + g_V^{eL} \mathcal{A}_2), \quad (B14)$$

with the arguments for the integral functions as $B(s, m_S^2, m_Z^2)$. The couplings are given in the following table:

S	g_{ZHWS}	g_{ZZS}
h^0	$-c_{\beta\alpha} / 2c_W$	$m_Z s_{\beta\alpha} / s_W c_W$
H^0	$s_{\beta\alpha} / 2c_W$	$m_Z c_{\beta\alpha} / s_W c_W$

$$\begin{aligned}
& + c_{\beta\alpha} s_W g_{H^-H^0G^+} (2B_1(k^2, m_{H^0}^2, m_W^2) + B_0(k^2, m_{H^0}^2, m_W^2)) \\
& - c_{\beta\alpha} s_{\beta\alpha} m_W (B_0(k^2, m_{h^0}^2, m_W^2) - B_1(k^2, m_{h^0}^2, m_W^2)) \\
& + c_{\beta\alpha} s_{\beta\alpha} m_W (B_0(k^2, m_{H^0}^2, m_W^2) - B_1(k^2, m_{H^0}^2, m_W^2)) .
\end{aligned} \tag{B17}$$

Fig. 3.4:

$$\begin{aligned}
\Sigma_{G^+H^+}^f(k^2) = & -\frac{N_c\alpha}{2\pi} \{ (y_{Htb}^L y_{Gtb}^R + y_{Htb}^R y_{Gtb}^L) A(m_t^2) + [m_b m_t (y_{Htb}^L y_{Gtb}^L + y_{Htb}^R y_{Gtb}^R) + m_b^2 (y_{Htb}^L y_{Gtb}^R + y_{Htb}^R y_{Gtb}^L)] B_0 \\
& + k^2 (y_{Htb}^L y_{Gtb}^R + y_{Htb}^R y_{Gtb}^L) B_1 \} ,
\end{aligned} \tag{B18}$$

with the arguments for the integral functions as $B(k^2, m_b^2, m_t^2)$.

Fig. 3.5 + 3.6:

$$\begin{aligned}
\Sigma_{G^+H^+}^b(k^2) = & \frac{\alpha}{4\pi} \{ g_{H^-h^0H^+} g_{H^-h^0G^+} B_0(k^2, m_{h^0}^2, m_{H^\pm}^2) + g_{H^-H^0H^+} g_{H^-H^0G^+} B_0(k^2, m_{H^0}^2, m_{H^\pm}^2) \\
& + g_{H^-h^0G^+} g_{G^-h^0G^+} B_0(k^2, m_{h^0}^2, m_W^2) + g_{H^-H^0G^+} g_{G^-H^0G^+} B_0(k^2, m_{H^0}^2, m_W^2) \\
& + \frac{s_{\beta\alpha} c_{\beta\alpha}}{4s_W^2} [-(k^2 + m_{h^0}^2) B_0(k^2, m_{h^0}^2, m_W^2) + 2k^2 B_1(k^2, m_{h^0}^2, m_W^2)] \\
& + \frac{s_{\beta\alpha} c_{\beta\alpha}}{4s_W^2} [(k^2 + m_{H^0}^2) B_0(k^2, m_{H^0}^2, m_W^2) - 2k^2 B_1(k^2, m_{H^0}^2, m_W^2)] \}
\end{aligned} \tag{B19}$$

Fig. 5.1: The real part of W^-H^- mixing self-energy fixes the counterterms for the γW^+H^- and ZW^+H^- vertices, following Eq. 14:

$$\mathcal{M} = \frac{4\pi\alpha}{s - m_V^2} g_V \text{Re}(\Sigma_{W^+H^+}(m_{H^\pm}^2)) (g_V^{eR} \mathcal{A}_1 + g_V^{eL} \mathcal{A}_2), \tag{B20}$$

where $g_\gamma = -1$, $g_Z = s_W/c_W$, and $\Sigma_{W^+H^+} = \Sigma_{W^+H^+}^f + \Sigma_{W^+H^+}^b = \text{Re}(\Sigma_{W^+H^+}) + i\text{Im}(\Sigma_{W^+H^+})$.

The W^-H^- counterterm cancels the real part of the W^-H^- mixing self-energy, following the renormalization condition defined in Eq. 13. Therefore, only the imaginary part of the W^-H^- mixing self-energy contributes to Figs. 5.2 and 5.3. Similarly, only the imaginary part of the G^-H^- mixing self-energy contributes to Fig. 5.4; this is related to the imaginary part of the W^-H^- mixing self-energy by Eq. 15.

Fig. 5.2:

$$\mathcal{M} = \frac{4\pi\alpha g_W^2}{m_{H^\pm}^2 - m_W^2} i\text{Im}(\Sigma_{W^+H^+}(m_{H^\pm}^2)) \mathcal{A}_2. \tag{B21}$$

Fig. 5.3:

$$\mathcal{M} = \frac{4\pi\alpha g_{VWW}}{(s - m_V^2)(m_{H^\pm}^2 - m_W^2)} (s - m_W^2) i\text{Im}(\Sigma_{W^+H^+}(m_{H^\pm}^2)) (g_V^{eR} \mathcal{A}_1 + g_V^{eL} \mathcal{A}_2), \tag{B22}$$

where $g_{\gamma WW} = -1$ and $g_{ZWW} = -c_W/s_W$.

Fig. 5.4:

$$\mathcal{M} = -\frac{4\pi\alpha g_{VWG} m_{H^\pm}^2}{(s - m_V^2)(m_{H^\pm}^2 - m_W^2) m_W} i\text{Im}(\Sigma_{W^+H^+}(m_{H^\pm}^2)) (g_V^{eR} \mathcal{A}_1 + g_V^{eL} \mathcal{A}_2), \tag{B23}$$

where $g_{\gamma WG} = m_W$ and $g_{ZWG} = -m_Z s_W$.

APPENDIX C: MSSM CONTRIBUTIONS

The matrix elements for $e^+e^- \rightarrow W^+H^-$ in the full MSSM are given here for the first time. The sfermion triangle that enters Fig. 2.2 was computed in Ref. [40], and agrees with our result. Fig. 2.1(b) with χ_i^0 , χ_j^0 and χ_k^+ in the loop is analogous to the top/bottom quark triangle

diagram and can be checked by substituting top/bottom quark couplings for the gaugino couplings; the part involving the W coupling to left-handed gauginos is consistent with the top/bottom quark contribution given in the previous section. Formulae were given in Ref. [33] for the W^+H^+ and G^+H^+ mixing diagrams, Fig. 4.1-4; our results are consistent with theirs, although not enough

detail was given in Ref. [33] to check the overall signs of the diagrams.

We define here our notation for the mixing matrices in the stop/sbottom and gaugino sectors and various coupling coefficients.

The mixing in stop sector is defined by:

$$\begin{pmatrix} \tilde{t}_L \\ \tilde{t}_R \end{pmatrix} = \begin{pmatrix} \cos \alpha_t \tilde{t}_1 - \sin \alpha_t \tilde{t}_2 \\ \sin \alpha_t \tilde{t}_1 + \cos \alpha_t \tilde{t}_2 \end{pmatrix}, \quad (\text{C1})$$

where $\tilde{t}_{L,R}$ are the weak eigenstates and $\tilde{t}_{1,2}$ are the mass

eigenstates, and analogously for the sbottom sector.

The chargino mass matrix is:

$$X = \begin{pmatrix} M_2 & \sqrt{2}m_W \sin \beta \\ \sqrt{2}m_W \cos \beta & \mu \end{pmatrix}, \quad (\text{C2})$$

which is diagonalized by the matrices U and V via $VX^\dagger U^\dagger = M_D$.

The neutralino mass matrix is:

$$Y = \begin{pmatrix} M_1 & 0 & -m_Z s_W \cos \beta & m_Z s_W \sin \beta \\ 0 & M_2 & m_Z c_W \cos \beta & -m_Z c_W \sin \beta \\ -m_Z s_W \cos \beta & m_Z c_W \cos \beta & 0 & -\mu \\ m_Z s_W \sin \beta & -m_Z c_W \sin \beta & -\mu & 0 \end{pmatrix}, \quad (\text{C3})$$

which is diagonalized by the matrix N via $NY^\dagger N^\dagger = N_D$.

The matrices that enter the $W^+ \chi_i^0 \chi_j^-$ couplings are defined as:

$$O_{ij}^L = -\frac{1}{\sqrt{2}}N_{i4}V_{j2}^* + N_{i2}V_{j1}^*, \quad O_{ij}^R = \frac{1}{\sqrt{2}}N_{i3}^*U_{j2} + N_{i2}^*U_{j1}. \quad (\text{C4})$$

The matrices that enter the $Z \chi_i^+ \chi_j^-$ couplings are defined as:

$$\begin{aligned} O_{ij}^L &= -V_{i1}V_{j1}^* - \frac{1}{2}V_{i2}V_{j2}^* + \delta_{ij}s_W^2, \\ O_{ij}^R &= -U_{i1}^*U_{j1} - \frac{1}{2}U_{i2}^*U_{j2} + \delta_{ij}s_W^2. \end{aligned} \quad (\text{C5})$$

The matrices that enter the $Z \chi_i^0 \chi_j^0$ couplings are de-

fined as:

$$O_{ij}^{\prime L} = -\frac{1}{2}N_{i3}N_{j3}^* + \frac{1}{2}N_{i4}N_{j4}^*, \quad O_{ij}^{\prime R} = -O_{ij}^{\prime L*}. \quad (\text{C6})$$

The matrices that enter the $H^- \chi_i^0 \chi_j^+$ couplings are defined as:

$$\begin{aligned} Q_{ij}^L &= N_{i4}^*V_{j1}^* + \frac{1}{\sqrt{2}}(N_{i2}^* + N_{i1}\tan\theta_W)V_{j2}^*, \\ Q_{ij}^R &= N_{i3}U_{j1} - \frac{1}{\sqrt{2}}(N_{i2} + N_{i1}\tan\theta_W)U_{j2}. \end{aligned} \quad (\text{C7})$$

The $H^- \tilde{f} \tilde{f}'$ coupling coefficients are given in the following table:

$g_{H\tilde{e}_L\tilde{\nu}}$	$-m_W \sin 2\beta/\sqrt{2}s_W$
$g_{H\tilde{d}_L\tilde{u}_L}$	$-m_W \sin 2\beta/\sqrt{2}s_W$
$g_{H-\tilde{b}_L\tilde{t}_L}$	$-m_W \sin 2\beta/\sqrt{2}s_W + (m_b^2 \tan \beta + m_t^2 \cot \beta)/\sqrt{2}m_W s_W$
$g_{H-\tilde{b}_L\tilde{t}_R}$	$m_t(\mu + A_t \cot \beta)/\sqrt{2}m_W s_W$
$g_{H-\tilde{b}_R\tilde{t}_L}$	$m_b(\mu + A_b \tan \beta)/\sqrt{2}m_W s_W$
$g_{H-\tilde{b}_R\tilde{t}_R}$	$m_t m_b(\tan \beta + \cot \beta)/\sqrt{2}m_W s_W$
$g_{H\tilde{b}_1\tilde{t}_1}$	$\cos \alpha_t \cos \alpha_b g_{H-\tilde{b}_L\tilde{t}_L} + \sin \alpha_t \cos \alpha_b g_{H-\tilde{b}_L\tilde{t}_R} + \cos \alpha_t \sin \alpha_b g_{H-\tilde{b}_R\tilde{t}_L} + \sin \alpha_t \sin \alpha_b g_{H-\tilde{b}_R\tilde{t}_R}$
$g_{H\tilde{b}_1\tilde{t}_2}$	$-\sin \alpha_t \cos \alpha_b g_{H-\tilde{b}_L\tilde{t}_L} + \cos \alpha_t \cos \alpha_b g_{H-\tilde{b}_L\tilde{t}_R} - \sin \alpha_t \sin \alpha_b g_{H-\tilde{b}_R\tilde{t}_L} + \cos \alpha_t \sin \alpha_b g_{H-\tilde{b}_R\tilde{t}_R}$
$g_{H\tilde{b}_2\tilde{t}_1}$	$-\cos \alpha_t \sin \alpha_b g_{H-\tilde{b}_L\tilde{t}_L} - \sin \alpha_t \sin \alpha_b g_{H-\tilde{b}_L\tilde{t}_R} + \cos \alpha_t \cos \alpha_b g_{H-\tilde{b}_R\tilde{t}_L} + \sin \alpha_t \cos \alpha_b g_{H-\tilde{b}_R\tilde{t}_R}$
$g_{H\tilde{b}_2\tilde{t}_2}$	$\sin \alpha_t \sin \alpha_b g_{H-\tilde{b}_L\tilde{t}_L} - \cos \alpha_t \sin \alpha_b g_{H-\tilde{b}_L\tilde{t}_R} - \sin \alpha_t \cos \alpha_b g_{H-\tilde{b}_R\tilde{t}_L} + \cos \alpha_t \cos \alpha_b g_{H-\tilde{b}_R\tilde{t}_R}$

The $G^- \tilde{f} \tilde{f}'$ coupling coefficients are given in the following table:

$g_{G\tilde{e}_L\tilde{\nu}}$	$m_W \cos 2\beta / \sqrt{2}s_W$
$g_{G\tilde{d}_L\tilde{u}_L}$	$m_W \cos 2\beta / \sqrt{2}s_W$
$g_{G-\tilde{b}_L\tilde{t}_L}$	$m_W \cos 2\beta / \sqrt{2}s_W + (m_t^2 - m_b^2) / \sqrt{2}m_W s_W$
$g_{G-\tilde{b}_L\tilde{t}_R}$	$m_t(-\mu \cot \beta + A_t) / \sqrt{2}m_W s_W$
$g_{G-\tilde{b}_R\tilde{t}_L}$	$-m_b(-\mu \tan \beta + A_b) / \sqrt{2}m_W s_W$
$g_{G-\tilde{b}_R\tilde{t}_R}$	0
$g_{G\tilde{b}_1\tilde{t}_1}$	$\cos \alpha_t \cos \alpha_b g_{G-\tilde{b}_L\tilde{t}_L} + \sin \alpha_t \cos \alpha_b g_{G-\tilde{b}_L\tilde{t}_R} + \cos \alpha_t \sin \alpha_b g_{G-\tilde{b}_R\tilde{t}_L}$
$g_{G\tilde{b}_1\tilde{t}_2}$	$- \sin \alpha_t \cos \alpha_b g_{G-\tilde{b}_L\tilde{t}_L} + \cos \alpha_t \cos \alpha_b g_{G-\tilde{b}_L\tilde{t}_R} - \sin \alpha_t \sin \alpha_b g_{G-\tilde{b}_R\tilde{t}_L}$
$g_{G\tilde{b}_2\tilde{t}_1}$	$- \cos \alpha_t \sin \alpha_b g_{G-\tilde{b}_L\tilde{t}_L} - \sin \alpha_t \sin \alpha_b g_{G-\tilde{b}_L\tilde{t}_R} + \cos \alpha_t \cos \alpha_b g_{G-\tilde{b}_R\tilde{t}_L}$
$g_{G\tilde{b}_2\tilde{t}_2}$	$\sin \alpha_t \sin \alpha_b g_{G-\tilde{b}_L\tilde{t}_L} - \cos \alpha_t \sin \alpha_b g_{G-\tilde{b}_L\tilde{t}_R} - \sin \alpha_t \cos \alpha_b g_{G-\tilde{b}_R\tilde{t}_L}$

We now list our results for the MSSM diagrams. It is to be understood that diagrams involving charginos χ_i^+ are summed over $i = 1, 2$ and diagrams involving neutralinos χ_i^0 are summed over $i = 1, \dots, 4$.

Fig. 2.1(a):

$$\begin{aligned}
\mathcal{M} = & -\frac{2\alpha^2}{s - m_V^2} \\
& \{ [(F - G + H)B_0 + (m_{\chi_k}^2(F - G + H) - k_1 \cdot k_2 H - m_{\chi_i} m_{\chi_j} m_{\chi_k} J)C_0 + (m_W^2 F + k_1 \cdot k_2 G - (k_1 \cdot k_2 - m_W^2)H)C_1 \\
& + (-k_1 \cdot k_2 F - m_{H^\pm}^2 G - (k_1 \cdot k_2 - m_{H^\pm}^2)H)C_2 - 2(F + H)C_{00}] (g_V^{eR} \mathcal{A}_1 + g_V^{eL} \mathcal{A}_2) \\
& + [H C_0 + (-G + H)C_1 + (F + 3H)C_2 + 2(F + H)(C_{12} + C_{22})] [g_V^{eR} (\mathcal{A}_3 + \mathcal{A}_5) + g_V^{eL} (\mathcal{A}_4 + \mathcal{A}_6)] \\
& + [H_{im} C_0 + (G_{im} + H_{im})C_1 + (F_{im} + H_{im})C_2] (g_V^{eR} \mathcal{A}_7 + g_V^{eL} \mathcal{A}_8) \}
\end{aligned} \quad (C8)$$

where

$$\begin{aligned}
F &= m_{\chi_i}(g_H^L g_V^L g_W^L + g_H^R g_V^R g_W^R), \quad G = m_{\chi_j}(g_H^L g_V^R g_W^L + g_H^R g_V^L g_W^R), \quad H = m_{\chi_k}(g_H^R g_V^L g_W^L + g_H^L g_V^R g_W^R), \\
J &= g_H^R g_V^R g_W^L + g_H^L g_V^L g_W^R, \\
F_{im} &= m_{\chi_i}(g_H^L g_V^L g_W^L - g_H^R g_V^R g_W^R), \quad G_{im} = m_{\chi_j}(g_H^L g_V^R g_W^L - g_H^R g_V^L g_W^R), \quad H_{im} = m_{\chi_k}(g_H^R g_V^L g_W^L - g_H^L g_V^R g_W^R). \quad (C9)
\end{aligned}$$

The arguments for the integral functions are $B(s, m_{\chi_j}^2, m_{\chi_i}^2)$, $C(m_W^2, s, m_{H^\pm}^2, m_{\chi_k}^2, m_{\chi_j}^2, m_{\chi_i}^2)$.

Fig. 2.1(b): Similar to Fig. 2.1(a), under the exchange of

$$g_H^L \leftrightarrow g_H^R, \quad \mathcal{A}_7, \mathcal{A}_8 \text{ terms flip sign.} \quad (C10)$$

The couplings are given in the following table:

	χ_i	χ_j	χ_k	g_γ^L	g_γ^R	g_Z^L	g_Z^R	g_H^L	g_H^R	g_W^L	g_W^R
2.1(a)	χ_i^+	χ_j^+	χ_k^0	$-\delta_{ij}$	$-\delta_{ij}$	O_{ji}^L/s_{WCW}	O_{ji}^R/s_{WCW}	$-Q_{ki}^{R*} \sin \beta / s_W$	$-Q_{ki}^{L*} \cos \beta / s_W$	O_{kj}^L/s_W	O_{kj}^R/s_W
2.1(b)	χ_i^0	χ_j^0	χ_k^+	0	0	$O_{ij}^{\prime L}/s_{WCW}$	$O_{ij}^{\prime R}/s_{WCW}$	$-Q_{ik}^{R*} \sin \beta / s_W$	$-Q_{ik}^{L*} \cos \beta / s_W$	O_{jk}^L/s_W	O_{jk}^R/s_W

Fig. 2.2:

$$\begin{aligned}
\mathcal{M} = & -\frac{4N_c\alpha^2}{s - m_V^2} g_{VS_iS_j} g_{HS_iS_k} g_{WS_jS_k} \{ C_{00} (g_V^{eR} \mathcal{A}_1 + g_V^{eL} \mathcal{A}_2) \\
& - (C_2 + C_{12} + C_{22}) [g_V^{eR} (\mathcal{A}_3 + \mathcal{A}_5) + g_V^{eL} (\mathcal{A}_4 + \mathcal{A}_6)] \} \}
\end{aligned} \quad (C11)$$

with the arguments for the integral functions as $C(m_W^2, s, m_{H^\pm}^2, m_{S_k}^2, m_{S_j}^2, m_{S_i}^2)$, $N_c = 1$ for sleptons and $N_c = 3$ for squarks. The couplings are given in the following table:

S_i	S_j	S_k	$g_{\gamma S_i S_j}$	$g_{Z S_i S_j}$	$g_{H S_i S_k}$	$g_{W S_j S_k}$
$\tilde{\nu}$	$\tilde{\nu}$	\tilde{e}_L	$-g_\gamma^{\nu L}$	$-g_Z^{\nu L}$	$g_{H\tilde{e}_L\tilde{\nu}}$	$-g_W$
\tilde{e}_L	\tilde{e}_L	$\tilde{\nu}$	g_γ^{eL}	g_Z^{eL}	$g_{H\tilde{e}_L\tilde{\nu}}$	g_W
\tilde{u}_L	\tilde{u}_L	\tilde{d}_L	$-g_\gamma^{uL}$	$-g_Z^{uL}$	$g_{H\tilde{d}_L\tilde{u}_L}$	$-g_W$
\tilde{d}_L	\tilde{d}_L	\tilde{u}_L	g_γ^{dL}	g_Z^{dL}	$g_{H\tilde{d}_L\tilde{u}_L}$	g_W
\tilde{t}_i	\tilde{t}_j	\tilde{b}_k	$-g_\gamma^{uL} M_{Li}^t M_{Lj}^t - g_\gamma^{uR} M_{Ri}^t M_{Rj}^t$	$-g_Z^{uL} M_{Li}^t M_{Lj}^t - g_Z^{uR} M_{Ri}^t M_{Rj}^t$	$g_{H\tilde{b}_k\tilde{t}_i}$	$-g_W M_{Lj}^t M_{Lk}^b$
\tilde{b}_i	\tilde{b}_j	\tilde{t}_k	$g_\gamma^{dL} M_{Li}^b M_{Lj}^b + g_\gamma^{dR} M_{Ri}^b M_{Rj}^b$	$g_Z^{dL} M_{Li}^b M_{Lj}^b + g_Z^{dR} M_{Ri}^b M_{Rj}^b$	$g_{H\tilde{b}_i\tilde{t}_k}$	$g_W M_{Lk}^t M_{Lj}^b$

where \tilde{t}_1 , \tilde{t}_2 , \tilde{b}_1 , \tilde{b}_2 are the stop and sbottom mass eigenstates, with mixing angle α_t , α_b , $M_{L1}^t = M_{R2}^t = \cos \alpha_t$, $-M_{L2}^t = M_{R1}^t = \sin \alpha_t$, $M_{L1}^b = M_{R2}^b = \cos \alpha_b$, $-M_{L2}^b = M_{R1}^b = \sin \alpha_b$.

Fig. 2.3:

$$\mathcal{M} = \alpha^2 g_W g_{\chi_i e \tilde{t}}^L g_{\chi_j \nu \tilde{t}}^R [(C_0 + C_2) m_{\chi_i} g_H^L + C_2 m_{\chi_j} g_H^R] \mathcal{A}_2, \quad (C12)$$

with the arguments for the integral functions as $C(0, u, m_{H^\pm}^2, m_{\chi_i}^2, m_{\tilde{t}}^2, m_{\chi_j}^2)$. The couplings are given in the following table:

χ_i	χ_j	\tilde{t}	g_H^L	g_H^R	$g_{\chi_i e \tilde{t}}^L$	$g_{\chi_j \nu \tilde{t}}^R$
χ_i^0	χ_j^+	\tilde{e}_L	$-Q'_{ij}^{R*} \sin \beta / s_W$	$-Q'_{ij}^{L*} \cos \beta / s_W$	$N_{i2}^* / \sqrt{2} s_W + N_{i1}^* / \sqrt{2} c_W$	$-U_{j1} / s_W$
χ_i^+	χ_j^0	$\tilde{\nu}$	$-Q'_{ji}^{R*} \sin \beta / s_W$	$-Q'_{ji}^{L*} \cos \beta / s_W$	$-V_{i1}^* / s_W$	$-N_{j2} / \sqrt{2} s_W + N_{j1} / \sqrt{2} c_W$

Fig. 2.4:

$$\mathcal{M} = -\alpha^2 g_W g_{\chi_i e \tilde{e}_L}^L g_{\chi_j \nu \tilde{\nu}}^R g_{H \tilde{e}_L \tilde{\nu}} C_2 \mathcal{A}_2, \quad (C13)$$

with the arguments for the integral functions as $C(0, u, m_{H^\pm}^2, m_{\tilde{e}_L}^2, m_{\chi_i}^2, m_{\tilde{\nu}}^2)$. The couplings are given in the following table:

χ_i	$g_{\chi_i e \tilde{e}_L}^L$	$g_{\chi_j \nu \tilde{\nu}}^R$
χ_i^0	$N_{i2}^* / \sqrt{2} s_W + N_{i1}^* / \sqrt{2} c_W$	$-N_{i2} / \sqrt{2} s_W + N_{i1} / \sqrt{2} c_W$

Fig. 2.5(a,c):

$$\begin{aligned} \mathcal{M} = & \alpha^2 g_{\chi_i e \tilde{t}}^L g_{\chi_k e \tilde{t}}^L \left\{ \left[m_{\chi_i} g_W^R g_H^L \left(-C_0 - m_{\chi_j}^2 D_0 - m_W^2 D_1 - u(D_2 + D_3) + 2D_{00} \right) \right. \right. \\ & + m_{\chi_j} g_W^R g_H^R \left(-C_0 - (u + m_{\chi_j}^2) D_0 - (u + m_W^2) D_1 - 2u D_2 - (u + m_{H^\pm}^2) D_3 + 2D_{00} \right) \\ & + m_{\chi_k} g_W^L g_H^R \left(C_0 + m_{\chi_j}^2 D_0 + u(D_1 + D_2) + m_{H^\pm}^2 D_3 \right) + m_{\chi_i} m_{\chi_j} m_{\chi_k} g_W^L g_H^L D_0 \Big] \mathcal{A}_2 \\ & + [m_{\chi_i} g_W^R g_H^L (-2(D_{33} + D_{13} + D_{23}) + m_{\chi_j} g_W^R g_H^R (-2D_3 - 2(D_{33} + D_{13} + D_{23}))) \Big] \mathcal{A}_4 \\ & + [m_{\chi_i} g_W^R g_H^L (-2(D_2 + D_3) - 2(D_{22} + D_{33} + D_{12} + D_{13} + D_{23})) \\ & + m_{\chi_j} g_W^R g_H^R (-2D_0 - (2D_1 + 4D_2 + 4D_3) - 2(D_{22} + D_{33} + D_{12} + D_{13} + 2D_{23})) \\ & \left. \left. + m_{\chi_k} g_W^L g_H^R 2D_1 \right] \mathcal{A}_6 \right\}, \end{aligned} \quad (C14)$$

with the arguments for the integral functions as $C(0, 0, s, m_{\chi_k}^2, m_{\tilde{t}}^2, m_{\chi_i}^2)$, $D(m_W^2, 0, 0, m_{H^\pm}^2, u, s, m_{\chi_j}^2, m_{\chi_k}^2, m_{\tilde{t}}^2, m_{\chi_i}^2)$. The couplings are given in the following table:

	χ_i	χ_j	χ_k	\tilde{t}	$g_{\chi_i e \tilde{t}}$	$g_{\chi_k e \tilde{t}}$	g_H^L	g_H^R	g_W^L	g_W^R
2.5(a)	χ_i^0	χ_j^+	χ_k^0	\tilde{e}_L	$\frac{N_{i2}^*}{\sqrt{2} s_W} + \frac{N_{i1}^*}{\sqrt{2} c_W}$	$\frac{N_{k2}}{\sqrt{2} s_W} + \frac{N_{k1}}{\sqrt{2} c_W}$	$-Q'_{ij}^{R*} \sin \beta / s_W$	$-Q'_{ij}^{L*} \cos \beta / s_W$	O_{kj}^L / s_W	O_{kj}^R / s_W
2.5(b)	χ_i^0	χ_j^+	χ_k^0	\tilde{e}_R	$-\sqrt{2} N_{i1} / c_W$	$-\sqrt{2} N_{k1}^* / c_W$	$-Q'_{ij}^{R*} \sin \beta / s_W$	$-Q'_{ij}^{L*} \cos \beta / s_W$	O_{kj}^L / s_W	O_{kj}^R / s_W
2.5(c)	χ_i^+	χ_j^0	χ_k^+	$\tilde{\nu}$	$-V_{i1}^* / s_W$	$-V_{k1} / s_W$	$-Q'_{ji}^{R*} \sin \beta / s_W$	$-Q'_{ji}^{L*} \cos \beta / s_W$	$-O_{jk}^R / s_W$	$-O_{jk}^L / s_W$
2.6(a)	χ_i^0	χ_j^+	χ_k^0	\tilde{e}_L	$\frac{N_{i2}^*}{\sqrt{2} s_W} + \frac{N_{i1}^*}{\sqrt{2} c_W}$	$\frac{N_{k2}}{\sqrt{2} s_W} + \frac{N_{k1}}{\sqrt{2} c_W}$	$-Q'_{ij}^{R*} \sin \beta / s_W$	$-Q'_{ij}^{L*} \cos \beta / s_W$	$-O_{ij}^R / s_W$	$-O_{ij}^L / s_W$
2.6(b)	χ_i^0	χ_j^+	χ_k^0	\tilde{e}_R	$-\sqrt{2} N_{i1} / c_W$	$-\sqrt{2} N_{k1}^* / c_W$	$-Q'_{kj}^{R*} \sin \beta / s_W$	$-Q'_{kj}^{L*} \cos \beta / s_W$	$-O_{ij}^R / s_W$	$-O_{ij}^L / s_W$

Fig. 2.5(b): Similar to Fig. 2.5(a,c), under the exchange of

$$g_H^L \leftrightarrow g_H^R, \quad g_W^L \leftrightarrow g_W^R, \quad \mathcal{A}_2 \leftrightarrow \mathcal{A}_1, \quad \mathcal{A}_4 \leftrightarrow \mathcal{A}_3, \quad \mathcal{A}_6 \leftrightarrow \mathcal{A}_5, \quad (C15)$$

Fig. 2.6(a):

$$\begin{aligned} \mathcal{M} = & \alpha^2 g_{\chi_i e \tilde{t}}^L g_{\chi_j e \tilde{t}}^L \left\{ \left[m_{\chi_i} g_W^L g_H^L \left(C_0 + m_{\chi_j}^2 D_0 + m_{H^\pm}^2 D_1 + t(D_2 + D_3) \right) \right. \right. \\ & + m_{\chi_j} g_W^R g_H^L \left(-C_0 - (m_{\chi_j}^2 + t) D_0 - (t + m_{H^\pm}^2) D_1 - 2t D_2 - (t + m_W^2) D_3 + 2D_{00} \right) \\ & + m_{\chi_k} g_W^R g_H^R \left(-C_0 - m_{\chi_j}^2 D_0 - t(D_1 + D_2) - m_W^2 D_3 + 2D_{00} \right) + m_{\chi_i} m_{\chi_j} m_{\chi_k} g_W^L g_H^R D_0 \Big] \mathcal{A}_2 \\ & + [m_{\chi_i} g_W^L g_H^L 2D_3 + m_{\chi_j} g_W^R g_H^L (-2D_0 - (4D_1 + 4D_2 + 2D_3) - 2(D_{11} + D_{22} + 2D_{12} + D_{13} + D_{23})) \\ & + m_{\chi_k} g_W^R g_H^R (-2(D_1 + D_2) - 2(D_{11} + D_{22} + 2D_{12} + D_{13} + D_{23})) \Big] \mathcal{A}_4 \\ & + [m_{\chi_j} g_W^R g_H^L (-2D_1 - 2(D_{11} + D_{12} + D_{13})) + m_{\chi_k} g_W^R g_H^R (-2)(D_{11} + D_{12} + D_{13})] \mathcal{A}_6 \Big\}, \end{aligned} \quad (C16)$$

with the arguments for the integral functions as $C(0, 0, s, m_{\chi_k}^2, m_{\tilde{l}}^2, m_{\chi_i}^2)$, $D(m_{H^\pm}^2, 0, 0, m_W^2, t, s, m_{\chi_j}^2, m_{\chi_k}^2, m_{\tilde{l}}^2, m_{\chi_i}^2)$.

Fig. 2.6(b): Similar to Fig. 2.6(a), under the exchange of

$$g_H^L \leftrightarrow g_H^R, \quad g_W^L \leftrightarrow g_W^R, \quad \mathcal{A}_2 \leftrightarrow \mathcal{A}_1, \quad \mathcal{A}_4 \leftrightarrow \mathcal{A}_3, \quad \mathcal{A}_6 \leftrightarrow \mathcal{A}_5, \quad (C17)$$

Fig. 2.7:

$$\begin{aligned} \mathcal{M} = & -2\alpha^2 g_{\chi_i e \tilde{e}_L}^L g_{\chi_i e \tilde{e}_L}^R g_{H \tilde{e}_L \tilde{\nu}} g_W [D_{00} \mathcal{A}_2 - (D_3 + D_{33} + D_{13} + D_{23}) \mathcal{A}_4 \\ & - (D_2 + D_3 + D_{22} + D_{33} + D_{12} + D_{13} + 2D_{23}) \mathcal{A}_6], \end{aligned} \quad (C18)$$

with the arguments for the integral functions as $D(m_W^2, 0, 0, m_{H^\pm}^2, u, s, m_{\tilde{\nu}}^2, m_{\tilde{e}_L}^2, m_{\chi_i}^2, m_{\tilde{e}_L}^2)$. The couplings are given in the following table:

χ_i	$g_{\chi_i e \tilde{e}_L}^L$	$g_{\chi_i e \tilde{e}_L}^R$
χ_i^0	$N_{i2}^*/\sqrt{2}s_W + N_{i1}^*/\sqrt{2}c_W$	$N_{i2}/\sqrt{2}s_W + N_{i1}/\sqrt{2}c_W$

Fig. 2.8:

$$\begin{aligned} \mathcal{M} = & -2\alpha^2 g_{\chi_i e \tilde{\nu}}^L g_{\chi_i e \tilde{\nu}}^R g_{H \tilde{e}_L \tilde{\nu}} g_W [D_{00} \mathcal{A}_2 - (D_1 + D_2 + D_{11} + D_{22} + 2D_{12} + D_{13} + D_{23}) \mathcal{A}_4 \\ & - (D_1 + D_{11} + D_{12} + D_{13}) \mathcal{A}_6], \end{aligned} \quad (C19)$$

where $D(m_{H^\pm}^2, 0, 0, m_W^2, t, s, m_{\tilde{e}_L}^2, m_{\tilde{\nu}}^2, m_{\chi_i}^2, m_{\tilde{\nu}}^2)$. The couplings are given in the following table:

χ_i	$g_{\chi_i e \tilde{\nu}}^L$	$g_{\chi_i e \tilde{\nu}}^R$
χ_i^+	$-V_{i1}^*/s_W$	$-V_{i1}/s_W$

Fig. 2.9:

$$\begin{aligned} \mathcal{M} = & -2\alpha^2 g_{\chi_i e \tilde{\nu}}^L g_{\chi_j e \tilde{e}_L}^R g_W \\ & \{ D_{00} (m_{\chi_i} g_H^L + m_{\chi_j} g_H^R) \mathcal{A}_2 + [(D_3 + D_{13} + D_{23}) m_{\chi_i} g_H^L + (D_{13} + D_{23}) m_{\chi_j} g_H^R] \mathcal{A}_4 \\ & + [-(D_2 + D_{12} + D_{22}) m_{\chi_i} g_H^L - (D_{12} + D_{22}) m_{\chi_j} g_H^R] \mathcal{A}_6 \}, \end{aligned} \quad (C20)$$

with the arguments for the integral functions as $D(m_W^2, 0, m_{H^\pm}^2, 0, u, t, m_{\tilde{\nu}}^2, m_{\tilde{e}_L}^2, m_{\chi_j}^2, m_{\chi_i}^2)$. The couplings are given in the following table:

χ_i	χ_j	g_H^L	g_H^R	$g_{\chi_i e \tilde{\nu}}^L$	$g_{\chi_j e \tilde{e}_L}^R$
χ_i^+	χ_j^0	$-Q_{ji}^{R*} \sin \beta / s_W$	$-Q_{ji}^{L*} \cos \beta / s_W$	$-V_{i1}^*/s_W$	$N_{j2}/\sqrt{2}s_W + N_{j1}/\sqrt{2}c_W$

Fig. 2.10:

$$\begin{aligned} \mathcal{M} = & \alpha^2 g_{\chi_i e \tilde{\nu}}^R g_{\chi_j e \tilde{e}_L}^L g_{H \tilde{e}_L \tilde{\nu}} \\ & \{ [m_{\chi_i} m_{\chi_j} g_W^L D_0 + g_W^R (-C_0 - m_{\chi_j}^2 D_0 - m_W^2 D_1 - u D_2 + 2D_{00})] \mathcal{A}_2 \\ & + 2g_W^R (D_{13} + D_{23}) \mathcal{A}_4 - 2g_W^R (D_2 + D_{12} + D_{22}) \mathcal{A}_6 \}, \end{aligned} \quad (C21)$$

with the arguments for the integrals as $C(0, m_{H^\pm}^2, t, m_{\chi_i}^2, m_{\tilde{\nu}}^2, m_{\tilde{e}_L}^2)$, $D(m_W^2, 0, m_{H^\pm}^2, 0, u, t, m_{\chi_j}^2, m_{\chi_i}^2, m_{\tilde{\nu}}^2, m_{\tilde{e}_L}^2)$. The couplings are given in the following table:

χ_i	χ_j	g_W^L	g_W^R	$g_{\chi_i e \tilde{\nu}}^R$	$g_{\chi_j e \tilde{e}_L}^L$
χ_i^+	χ_j^0	$-O_{ji}^R/s_W$	$-O_{ji}^L/s_W$	$-V_{i1}/s_W$	$N_{j2}^*/\sqrt{2}s_W + N_{j1}^*/\sqrt{2}c_W$

Fig. 2.11:

$$\mathcal{M} = \frac{N_c \alpha^2}{s - m_V^2} g_{VWS_i S_j} g_{HS_i S_j} B_0 (g_V^{eR} \mathcal{A}_1 + g_V^{eL} \mathcal{A}_2), \quad (C22)$$

with the arguments for the integral functions as $B(m_{H^\pm}^2, m_{S_j}^2, m_{S_i}^2)$, $N_c = 1$ for sleptons and $N_c = 3$ for squarks. The couplings are given in the following table:

S_i	S_j	$g_{HS_iS_j}$	$g_{\gamma WS_iS_j}$	$g_{ZWS_iS_j}$
$\tilde{\nu}$	\tilde{e}_L	$g_{H\tilde{e}_L\tilde{\nu}}$	$(e_e + e_\nu)/\sqrt{2}s_W$	$-(e_e + e_\nu)/\sqrt{2}c_W$
\tilde{u}_L	\tilde{d}_L	$g_{H\tilde{d}_L\tilde{u}_L}$	$(e_u + e_d)/\sqrt{2}s_W$	$-(e_u + e_d)/\sqrt{2}c_W$
\tilde{t}_1	\tilde{b}_1	$g_{H\tilde{b}_1\tilde{t}_1}$	$(e_u + e_d) \cos \alpha_t \cos \alpha_b/\sqrt{2}s_W$	$-(e_u + e_d) \cos \alpha_t \cos \alpha_b/\sqrt{2}c_W$
\tilde{t}_1	\tilde{b}_2	$g_{H\tilde{b}_2\tilde{t}_1}$	$-(e_u + e_d) \cos \alpha_t \sin \alpha_b/\sqrt{2}s_W$	$(e_u + e_d) \cos \alpha_t \sin \alpha_b/\sqrt{2}c_W$
\tilde{t}_2	\tilde{b}_1	$g_{H\tilde{b}_1\tilde{t}_2}$	$-(e_u + e_d) \sin \alpha_t \cos \alpha_b/\sqrt{2}s_W$	$(e_u + e_d) \sin \alpha_t \cos \alpha_b/\sqrt{2}c_W$
\tilde{t}_2	\tilde{b}_2	$g_{H\tilde{b}_2\tilde{t}_2}$	$(e_u + e_d) \sin \alpha_t \sin \alpha_b/\sqrt{2}s_W$	$-(e_u + e_d) \sin \alpha_t \sin \alpha_b/\sqrt{2}c_W$

Fig. 4.1:

$$\Sigma_{W^+H^+}^f(k^2) = \frac{\alpha}{2\pi} \{ [m_{\chi_j}(g_H^L g_W^L + g_H^R g_W^R) + m_{\chi_i}(g_H^L g_W^R + g_H^R g_W^L)] B_1 + m_{\chi_i}(g_H^L g_W^R + g_H^R g_W^L) B_0 \}, \quad (C23)$$

with the arguments for the integral functions as $B(k^2, m_{\chi_i}^2, m_{\chi_j}^2)$, for k being the external momentum. The couplings are given in the following table:

χ_i	χ_j	g_H^L	g_H^R	g_W^L	g_W^R
χ_i^0	χ_j^+	$-Q_{ij}^{LR*} \sin \beta/s_W$	$-Q_{ij}^{LL*} \cos \beta/s_W$	O_{ij}^L/s_W	O_{ij}^R/s_W

Fig. 4.2:

$$\Sigma_{W^+H^+}^b(k^2) = -\frac{N_c \alpha}{4\pi} g_{HS_iS_j} g_{WS_iS_j} (2B_1 + B_0), \quad (C24)$$

with the arguments for the integral functions as $B(k^2, m_{S_j}^2, m_{S_i}^2)$, for k being the external momentum. The couplings are given in the following table:

S_i	S_j	$g_{HS_iS_j}$	$g_{WS_iS_j}$
$\tilde{\nu}$	\tilde{e}_L	$g_{H\tilde{e}_L\tilde{\nu}}$	g_W
\tilde{u}_L	\tilde{d}_L	$g_{H\tilde{d}_L\tilde{u}_L}$	g_W
\tilde{t}_1	\tilde{b}_1	$g_{H\tilde{b}_1\tilde{t}_1}$	$g_W \cos \alpha_t \cos \alpha_b$
\tilde{t}_1	\tilde{b}_2	$g_{H\tilde{b}_2\tilde{t}_1}$	$-g_W \cos \alpha_t \sin \alpha_b$
\tilde{t}_2	\tilde{b}_1	$g_{H\tilde{b}_1\tilde{t}_2}$	$-g_W \sin \alpha_t \cos \alpha_b$
\tilde{t}_2	\tilde{b}_2	$g_{H\tilde{b}_2\tilde{t}_2}$	$g_W \sin \alpha_t \sin \alpha_b$

Fig. 4.3:

$$\begin{aligned} \Sigma_{G^+H^+}^f(k^2) = & -\frac{\alpha}{2\pi} \{ (g_H^L g_G^R + g_H^R g_G^L) A(m_{\chi_j}^2) + [m_{\chi_i}^2 (g_H^L g_G^R + g_H^R g_G^L) + m_{\chi_i} m_{\chi_j} (g_H^L g_G^L + g_H^R g_G^R)] B_0 \\ & + k^2 (g_H^L g_G^R + g_H^R g_G^L) B_1 \}, \end{aligned} \quad (C25)$$

with the arguments for the integral functions as $B(k^2, m_{\chi_i}^2, m_{\chi_j}^2)$, for k being the external momentum. The couplings are given in the following table:

χ_i	χ_j	g_H^L	g_H^R	g_G^L	g_G^R
χ_i^0	χ_j^+	$-Q_{ij}^{LR*} \sin \beta/s_W$	$-Q_{ij}^{LL*} \cos \beta/s_W$	$-Q_{ij}^L \sin \beta/s_W$	$Q_{ij}^R \cos \beta/s_W$

Fig. 4.4:

$$\Sigma_{G^+H^+}^b(k^2) = \frac{N_c \alpha}{4\pi} g_{HS_iS_j} g_{GS_iS_j} B_0, \quad (C26)$$

with the arguments for the integral functions as $B(k^2, m_{S_j}^2, m_{S_i}^2)$, for k being the external momentum. The couplings are given in the following table:

S_i	S_j	$g_{HS_iS_j}$	$g_{GS_iS_j}$
$\tilde{\nu}$	\tilde{e}_L	$g_{H\tilde{e}_L\tilde{\nu}}$	$g_{G\tilde{e}_L\tilde{\nu}}$
\tilde{u}_L	\tilde{d}_L	$g_{H\tilde{d}_L\tilde{u}_L}$	$g_{G\tilde{d}_L\tilde{u}_L}$
\tilde{t}_1	\tilde{b}_1	$g_{H\tilde{b}_1\tilde{t}_1}$	$g_{G\tilde{b}_1\tilde{t}_1}$
\tilde{t}_1	\tilde{b}_2	$g_{H\tilde{b}_2\tilde{t}_1}$	$g_{G\tilde{b}_2\tilde{t}_1}$
\tilde{t}_2	\tilde{b}_1	$g_{H\tilde{b}_1\tilde{t}_2}$	$g_{G\tilde{b}_1\tilde{t}_2}$
\tilde{t}_2	\tilde{b}_2	$g_{H\tilde{b}_2\tilde{t}_2}$	$g_{G\tilde{b}_2\tilde{t}_2}$

[1] J. F. Gunion, H. E. Haber, G. L. Kane and S. Dawson, *The Higgs Hunter's Guide*, (Perseus Publishing, Cambridge, MA, 2000).

[2] J. F. Gunion and H. E. Haber, Nucl. Phys. B **272**, 1 (1986) [Erratum B **402**, 567 (1986)]; B **278**, 449 (1986).

[3] J. Dai, J. F. Gunion and R. Vega, Phys. Lett. B **387**, 801 (1996).

[4] C. Balazs, J. L. Diaz-Cruz, H. J. He, T. Tait and C. P. Yuan, Phys. Rev. D **59**, 055016 (1999).

[5] M. Carena *et al.*, Report of the Tevatron Higgs working group, arXiv:hep-ph/0010338.

[6] M. Carena, S. Mrenna and C. E. M. Wagner, Phys. Rev. D **60**, 075010 (1999).

[7] A. Belyaev, D. Garcia, J. Guasch and J. Sola, arXiv:hep-ph/0203031.

[8] M. Guchait and S. Moretti, JHEP **0201**, 001 (2002).

[9] K. Lassila-Perini, ETH Dissertation thesis No. 12961 (1998); ATLAS collaboration Technical Design Report, available from <http://atlasinfo.cern.ch/Atlas/GROUPS/PHYSICS/TDR/access.html>.

[10] D. Denegri *et al.*, arXiv:hep-ph/0112045.

[11] K. A. Assamagan, Y. Coadou and A. Deandrea, arXiv:hep-ph/0203121; K. A. Assamagan and Y. Coadou, Acta Phys. Polon. B **33**, 707 (2002).

[12] LEP Higgs Working Group Collaboration, arXiv:hep-ex/0107030.

[13] A. Kiiskinen, M. Battaglia and P. Pöyhönen, in *Physics and experiments with future linear e^+e^- colliders*, Proc. of the 5th Int. Linear Collider Workshop, Batavia, Illinois, USA, 2000, edited by A. Para and H. E. Fisk (American Institute of Physics, New York, 2001), pp. 237-240 [arXiv:hep-ph/0101239].

[14] A. Andreazza and C. Troncon, "Study of HA Production in e^+e^- Collisions at $\sqrt{s} = 800$ GeV", DESY-123-E, p. 417, and in J. A. Aguilar-Saavedra *et al.* [ECFA/DESY LC Physics Working Group], *TESLA Technical Design Report, Part 3: Physics at an e^+e^- linear collider* [hep-ph/0106315].

[15] D. Zeppenfeld, R. Kinnunen, A. Nikitenko and E. Richter-Was, Phys. Rev. D **62**, 013009 (2000).

[16] M. Battaglia and K. Desch, in *Physics and experiments with future linear e^+e^- colliders*, Proc. of the 5th Int. Linear Collider Workshop, Batavia, Illinois, USA, 2000, edited by A. Para and H. E. Fisk (American Institute of Physics, New York, 2001), pp. 163-182 [hep-ph/0101165].

[17] J. A. Aguilar-Saavedra *et al.* [ECFA/DESY LC Physics Working Group], *TESLA Technical Design Report, Part 3: Physics at an e^+e^- linear collider* [hep-ph/0106315].

[18] T. Abe *et al.* [American Linear Collider Working Group Collaboration], *Linear collider physics resource book for Snowmass 2001, Part 2: Higgs and supersymmetry studies*, hep-ex/0106056.

[19] H. E. Haber and Y. Nir, Nucl. Phys. B **335**, 363 (1990); H. E. Haber, in *Physics From the Planck Scale to the Electroweak Scale*, Proceedings of the US-Polish Workshop, Warsaw, Poland, 1994, edited by P. Nath, T. Taylor, and S. Pokorski (World Scientific, Singapore, 1995), pp. 49-63, hep-ph/9501320.

[20] M. Carena, H. E. Haber, H. E. Logan and S. Mrenna, Phys. Rev. D **65**, 055005 (2002).

[21] M. M. Velasco *et al.*, in *Proc. of the APS/DPF/DPB Summer Study on the Future of Particle Physics (Snowmass 2001)* ed. R. Davidson and C. Quigg, arXiv:hep-ex/0111055; D. Asner *et al.*, arXiv:hep-ex/0111056.

[22] S. Heinemeyer, W. Hollik, J. Rosiek and G. Weiglein, Eur. Phys. J. C **19**, 535 (2001); see www.feynhiggs.de.

[23] M. Carena, H. E. Haber, S. Heinemeyer, W. Hollik, C. E. Wagner and G. Weiglein, Nucl. Phys. B **580**, 29 (2000).

[24] M. Berggren, R. Keranen and A. Sopczak, Eur. Phys. J. direct C **8**, 1 (2000); J. F. Gunion, T. Han, J. Jiang, S. Mrenna and A. Sopczak, in *Proc. of the APS/DPF/DPB Summer Study on the Future of Particle Physics (Snowmass 2001)* ed. R. Davidson and C. Quigg, arXiv:hep-ph/0112334.

[25] A. Gutierrez-Rodriguez, M. A. Hernandez-Ruiz and O. A. Sampayo, arXiv:hep-ph/0110289.

[26] U. Cotti, A. Gutierrez-Rodriguez, A. Rosado and O. A. Sampayo, Phys. Rev. D **59**, 095011 (1999).

[27] S. Kanemura, S. Moretti and K. Odagiri, JHEP **0102**, 011 (2001).

[28] A. Gutierrez-Rodriguez and O. A. Sampayo, Phys. Rev. D **62**, 055004 (2000).

[29] H. J. He, S. Kanemura and C. P. Yuan, arXiv:hep-ph/0203090.

[30] D. M. Asner, J. B. Gronberg and J. F. Gunion, arXiv:hep-ph/0110320.

[31] M. M. Mühlleitner, M. Kramer, M. Spira and P. M. Zerwas, Phys. Lett. B **508**, 311 (2001).

[32] J. F. Gunion and H. E. Haber, Phys. Rev. D **48**, 5109 (1993).

[33] F. Zhou, W. G. Ma, Y. Jiang, X. Q. Li and L. H. Wan, Phys. Rev. D **64**, 055005 (2001).

[34] A. Mendez and A. Pomarol, Phys. Lett. B **272**, 313 (1991); J. F. Gunion, H. E. Haber and C. Kao, Phys. Rev. D **46**, 2907 (1992).

[35] A. G. Akeroyd, A. Arhrib and M. Capdequi Peyranère, Mod. Phys. Lett. A **14**, 2093 (1999).

[36] A. G. Akeroyd, A. Arhrib and M. Capdequi Peyranère, Phys. Rev. D **64**, 075007 (2001).

[37] A. Arhrib, private communication.

[38] A. Djouadi, V. Driesen, W. Hollik and J. Rosiek, Nucl. Phys. B **491**, 68 (1997).

[39] T. Farris, J. F. Gunion and H. E. Logan, in *Proc. of the APS/DPF/DPB Summer Study on the Future of Particle Physics (Snowmass 2001)* ed. R. Davidson and C. Quigg, arXiv:hep-ph/0202087.

[40] M. Capdequi Peyranère, H. E. Haber and P. Irulegui, Phys. Rev. D **44**, 191 (1991).

[41] S. Kanemura, Phys. Rev. D **61**, 095001 (2000).

[42] P. Irulegui Gomes, *Charged Higgs Decay into W-Photon and W-Z in the Minimal Supersymmetric Model*, Ph.D. Thesis, SCIPP-91/15 (1991).

[43] A. Mendez and A. Pomarol, Nucl. Phys. B **349**, 369 (1991).

[44] S. Kanemura and K. Odagiri, arXiv:hep-ph/0104179.

[45] For the TESLA design, see, *e.g.*: http://www.desy.de/~njwalker/ecfa-desy-wg4/parameter_list.html.

[46] A. Arhrib, M. Capdequi Peyranère, W. Hollik and G. Mouttaka, Nucl. Phys. B **581**, 34 (2000).

[47] S. Kanemura, Eur. Phys. J. C **17**, 473 (2000).

- [48] S. H. Zhu, arXiv:hep-ph/9901221.
- [49] P. Breitenlohner and D. Maison, Commun. Math. Phys. **52**, 11 (1977); **52**, 39 (1977); **52**, 55 (1977).
- [50] G. Bonneau, Phys. Lett. B **96**, 147 (1980); Nucl. Phys. B **177**, 523 (1981); D. Maison, Phys. Lett. B **150**, 139 (1985).
- [51] G. 't Hooft and M. J. Veltman, Nucl. Phys. B **44**, 189 (1972); D. A. Akyeampong and R. Delbourgo, Nuovo Cim. A **17**, 578 (1973); **18**, 94 (1973); **19**, 219 (1974).
- [52] A. J. Buras and P. H. Weisz, Nucl. Phys. B **333**, 66 (1990).
- [53] A. Dabelstein, Z. Phys. C **67**, 495 (1995).
- [54] J. A. Coarasa, D. Garcia, J. Guasch, R. A. Jimenez and J. Sola, Eur. Phys. J. C **2**, 373 (1998).
- [55] M. Capdequi Peyranère, Int. J. Mod. Phys. A **14**, 429 (1999).
- [56] H. E. Logan and S. Su, in preparation.
- [57] T. Farris, J. F. Gunion, H. E. Logan and S. Su, in preparation.
- [58] H. E. Haber and G. L. Kane, Phys. Rept. **117**, 75 (1985).